HYDRODYNAMIC MODELING OF DISPERSION AND DILUTION OF CONCENTRATED SEAWATER PRODUCED BY THE OCEAN DESALINATION PROJECT AT THE ENCINA POWER PLANT, CARLSBAD, CA, PART II : SALINE ANOMALIES DUE TO THEORETICAL EXTREME CASE HYDRAULIC SCENARIOS

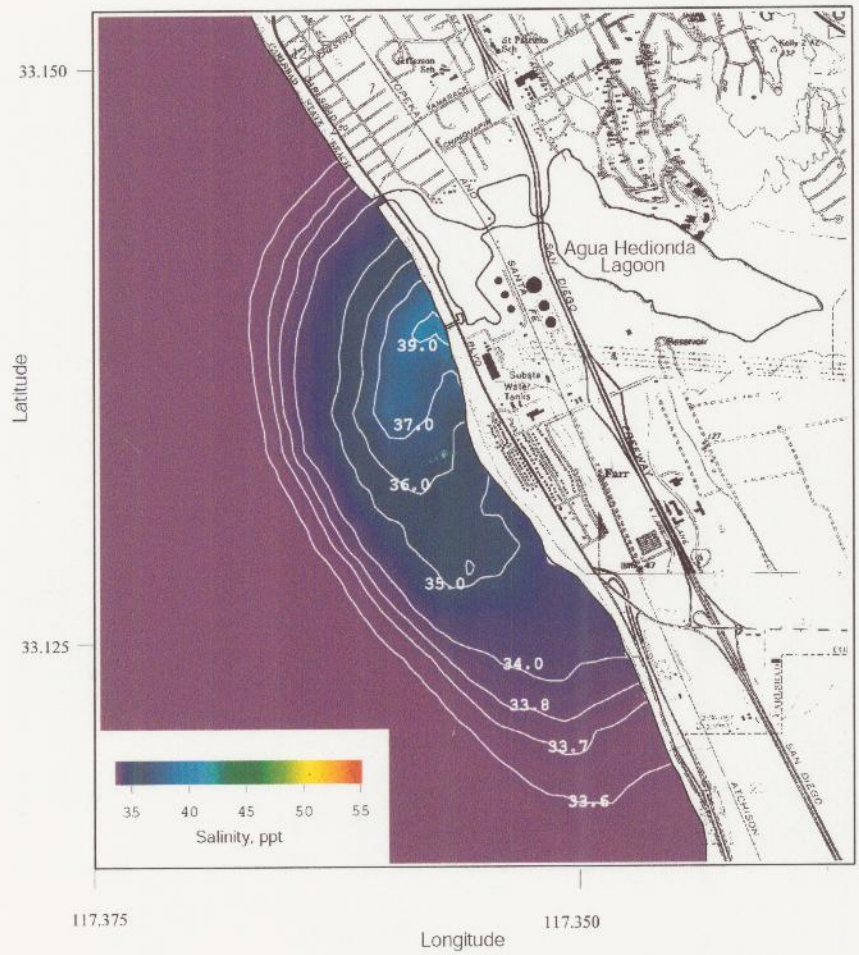

Submitted by:
Scott A. Jenkins, Ph. D. and Joseph Wasyl
Dr. Scott A. Jenkins Consulting
14765 Kalapana Street, Poway, CA 92064

Submitted to:
Poseidon Resources
501 West Broadway, San Diego, CA 92101

Revised : 7 March 2005

TABLE OF CONTENTS

TABLE OF CONTENTS (continued)

HYDRODYNAMIC MODELING OF DISPERSION AND DILUTION OF CONCENTRATED SEAWATER PRODUCED BY THE OCEAN DESALINATION PROJECT AT THE ENCINA POWER PLANT, CARLSBAD, CA

by

Scott A. Jenkins, Ph. D. and Joseph Wasyl

Executive Summary

Poseidon Resources plans to construct and operate a reverse osmosis (RO) desalination plant at the Encina Power Plant in Carlsbad, CA. This proposed project is referred to as the ***Carlsbad Desalination Project.*** Fifty million gallons per day (mgd) of treated water from this plant will be blended with other supplies to provide supplemental water to the City of Carlsbad, and/or other agencies. The source of water for the desalination plant will be seawater drawn from the Agua Hedionda Lagoon after passing through the power plant's cooling water condensers. The source water will be pre-treated and filtered through reverse osmosis membranes to produce high quality drinking water. The drinking water will be distributed to nearby water agencies. The concentrated seawater byproduct of the reverse osmosis process will be mixed with the cooling water and then conveyed to the existing outfall channel.

This is Part II of a hydrodynamic modeling study of the nearshore waters adjacent to the Encina Power Plant that was conducted to evaluate the mixing and dilution of the concentrated byproduct of the desalination process with its

associated thermal plume after it is returned to the cooling water discharge from the power plant. In Part I the model was initialized for four sets of average and extreme environmental conditions: 1) an historical extreme day, 2) an historical average day, 3) an historical extreme month, and 4) an historical average month. The concepts of extreme and average case apply to the simultaneous occurrence of 7 boundary condition and forcing function variables that in combination control acute and chronic toxicity tendencies for the combined RO and power plant discharge. These 7 variables include: ocean temperatures and salinities, ocean water levels (tides plus sea level anomalies), power plant flow rates, wind, waves, and currents. These variables control the concentrations and persistence of elevated salinities and temperatures associated with the combined discharge.

The Part I analysis developed historic surrogates for extreme and average case combinations of these 7 controlling variables that were then used to assess saline and thermal impacts of the proposed desalination project. It was found that saline impacts were largest on the sea floor, but were elevated by less than 10 % in existing benthic habitat areas when RO production was limited to 50 mgd. The addition of concentrated seawater from desalination to the thermal discharge of the power plant renders the combined discharge heavier than ambient seawater at all levels of power plant and RO operating conditions. However, this modification to the buoyant properties of the thermal effluent was not found to cause any violations to either the Section 316(A) provisions of the existing NPDES permit or relevant sections of California's Thermal Plan dealing with Specific Water Quality Objectives, General Water Quality Provisions. In fact, the addition of concentrated seawater to the discharge stream was found to result in a reduction of between 50%

and 86% in the thermal footprint relative to existing conditions. One particular water quality objective of The Thermal Plan is used as a diagnostic for the extreme cases in Part II . That standard is set forth in Water Quality Objective 3B(4) and defines a ***zone of initial dilution (ZID)*** extending 1000 feet in any direction from the discharge channel. Although all of the 50 mgd scenarios of the Part I analysis satisfy the dilution and thermal requirements for the ZID, some of those studied in Part II do not.

Here in Part II we revisit the Part I analysis with some additional "extreme case" scenarios that involve some potential situations for operating the desalination plant when the power plant is not generating electricity or when it is operating at very low production levels that are either rare or atypical of the long-term historic operating record. We refer to these as "historical extreme cases" because they are caused by extreme conditions occurring "in-the-pipe" in combination with extreme conditions in the ocean environment. The extreme in-the-pipe conditions are due to either low power plant flow rate or no heating of the discharge water because the power plant is out of service. (The latter is referred to as " ***Zero Delta-T"*** , $\Delta T = 0$, where ΔT is the temperature difference between ocean water and plant discharge). In the present study, these historical extreme conditions are superimposed on the historic extreme combinations of the remaining 6 controlling variables used previously in the Part I study. The resulting modeled response gives the expected impacts for a set of historical extreme cases that can not be reproduced from the historic records of all 7 controlling variables during last two decades (1980- July 2000). To establish a statistical comparison for these historical extreme cases, we find 7523 alternative solutions for the modeled ocean response to the 50 mgd

desalination plant, based on historically realized plant operations and ocean conditions.

We evaluated 2 historical extreme case scenarios from which the desalination plant might extract its source water: 1) ***Unheated Unit 4 Historical Extreme Case*** with two circulation pumps and service water operating at a flow rate of 304 mgd and $\Delta T = 0$ °C; and, 2) ***Heated Unit 4 Historical Extreme Case*** with two circulation pumps and service water yielding a flow rate of 304 mgd and $\Delta T = 5.5$ °C. These historical extreme cases are contrasted against the historical average operating conditions with various combinations of pumps and service water producing 576 mgd of heated discharge $\Delta T = 5.5$ °C.

The analysis of these historical extreme case scenarios employed the ***SEDXPORT*** modeling system that was developed at Scripps Institution of Oceanography for the US Navy's *Coastal Water Clarity System* and *Littoral Remote Sensing Simulator*. This model has been peer reviewed multiple times and has been calibrated and validated in the Southern California Bight for 4 previous desalination design projects.

Results for the historical extreme case scenarios are summarized in Table E-1 in terms of the maximum salinities and minimum dilution factors found on the sea floor and in the water column along the outer edge of the zone of initial dilution (ZID), 1000 feet from the end of the discharge channel. In all cases the maximum salinities are found on the sea floor directly offshore of the discharge channel as illustrated in Figure E-1. Maximum salinities in the water column are found in the surf zone, down-drift from the discharge channel to the south. We find that both heated and unheated water discharges for the Unit 4 historical

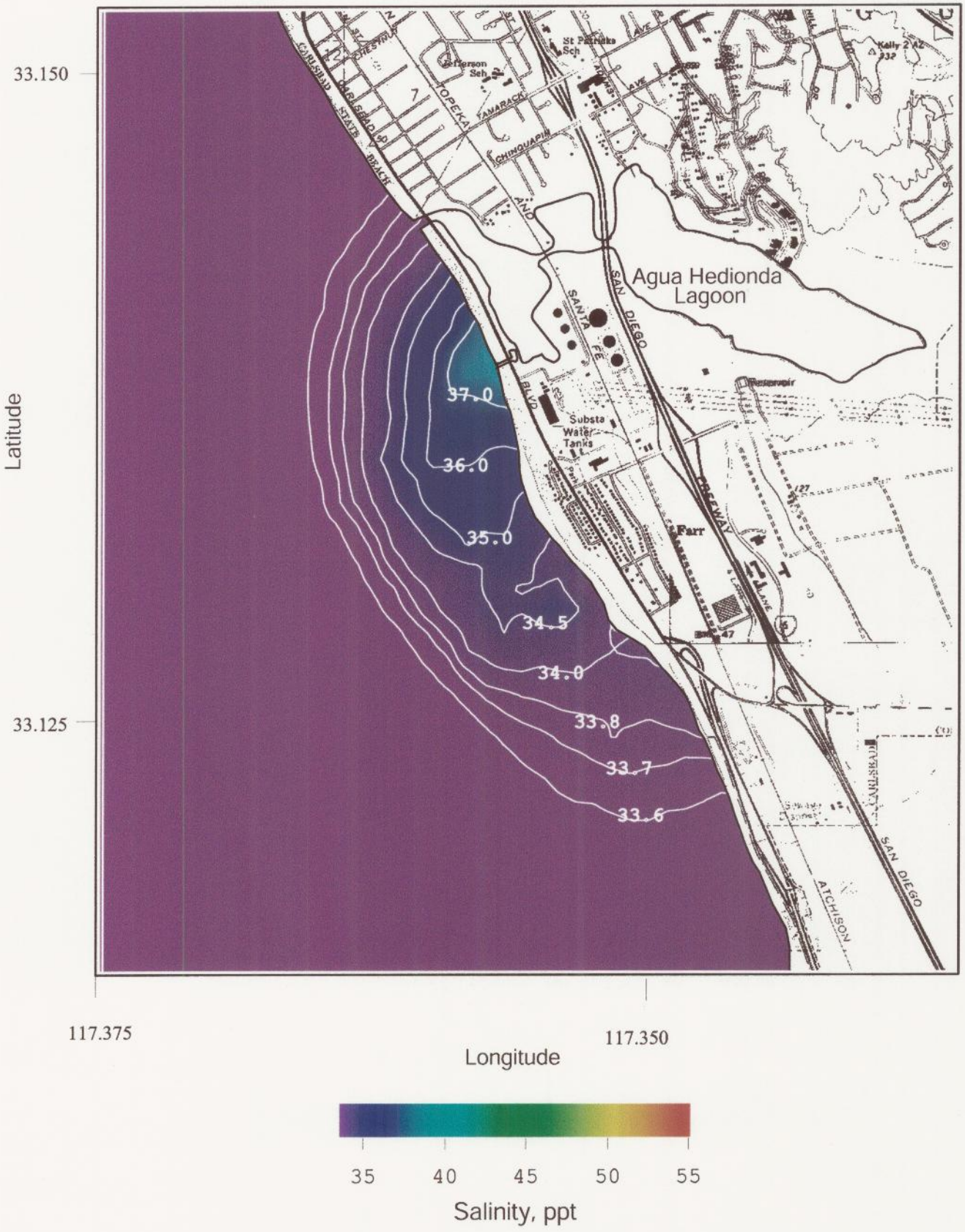

Figure E-1. Historical extreme conditions for Unit 4 with 2 pumps, heated ($\Delta T = 5.5\ ^{o}C$). Daily average of the bottom salinity of concentrated seawater for R.O. = 50 mgd, plant inflow rate = 304 mgd, combined discharge = 254 mgd, ambient ocean salinity = 33.51 ppt, ocean conditions, 17 Aug 1992.

extreme scenarios appear to give acceptable dilution factors at the ZID ranging from 19.8 to 1 for the unheated discharges ($\Delta T = 0$ °C), increasing to 24.1 to 1 for the heated discharges ($\Delta T = 5.5$ °C). For historical average power plant operating conditions with heated discharge, the dilution of the concentrated seawater from

Table E-1. Summary of historical extreme case scenarios: salinity and dilution factors 1000 ft. from the discharge (outer edge of the zone of initial dilution, ZID).

Scenario	Plant Inflow rate (mgd)	Bottom salinity (ppt)	Bottom Dilution Factor	Water Column Salinity (ppt)	Water Column Dilution Factor
Unit 4 Historical Extreme (2 pumps, unheated)	304 ($\Delta T = 0$ °C)	38.2	7.1 to 1	35.2	19.8 to 1
Unit 4 Historical Extreme (2 pumps, heated)	304 ($\Delta T = 5.5$ °C)	36.3	12.0 to 1	34.9	24.1 to 1
Historical Average (variable pumps, heated)	576 ($\Delta T = 5.5$ °C)	34.4	37.7 to 1	34.0	68.4 to 1

desalination is significantly higher than these historical extreme cases, reaching a minimum of 68.4 to 1 at the ZID.

The model was run on 20.5 years of continuous historic data from the period 1980-July 2000. Figure E-2 shows that maximum bottom salinity at the ZID varies from a minimum of 33 ppt to as high as 38.2 ppt, with a median value of 34.4 ppt (average ocean salinity is 33.5 ppt and seasonal maximum is 34.44). Figure E-2 indicates that 95% of the time salinity at the edge of the ZID is less than 36.2 ppt and will never exceed 38.2 ppt, the Unit-4 limit for extreme historical cases. Because the concentrated seawater from desalination is heavier than ambient seawater, these bottom salinities represent the highest possible values found anywhere in the local marine environment during historical variability. In the middle of the ZID, only 500 ft from the discharge channel, the maximum sea floor salinities would remain less than 39.3 ppt for all possible outcomes within the realm of historical variability in ocean and power plant operating conditions. Figure E-3 shows that the potential range of minimum bottom dilution at the ZID goes as high as 96 to 1, and as low as 8 to 1, depending on the historical combinations of power plant operations and ocean mixing levels. Only 7 % of the potential outcomes produce dilutions of less than 15 to 1 at the edge of the ZID. The unheated Unit 4 historical extreme case for 304 mgd, gives a minimum bottom dilution at the ZID of 7.1 to 1.

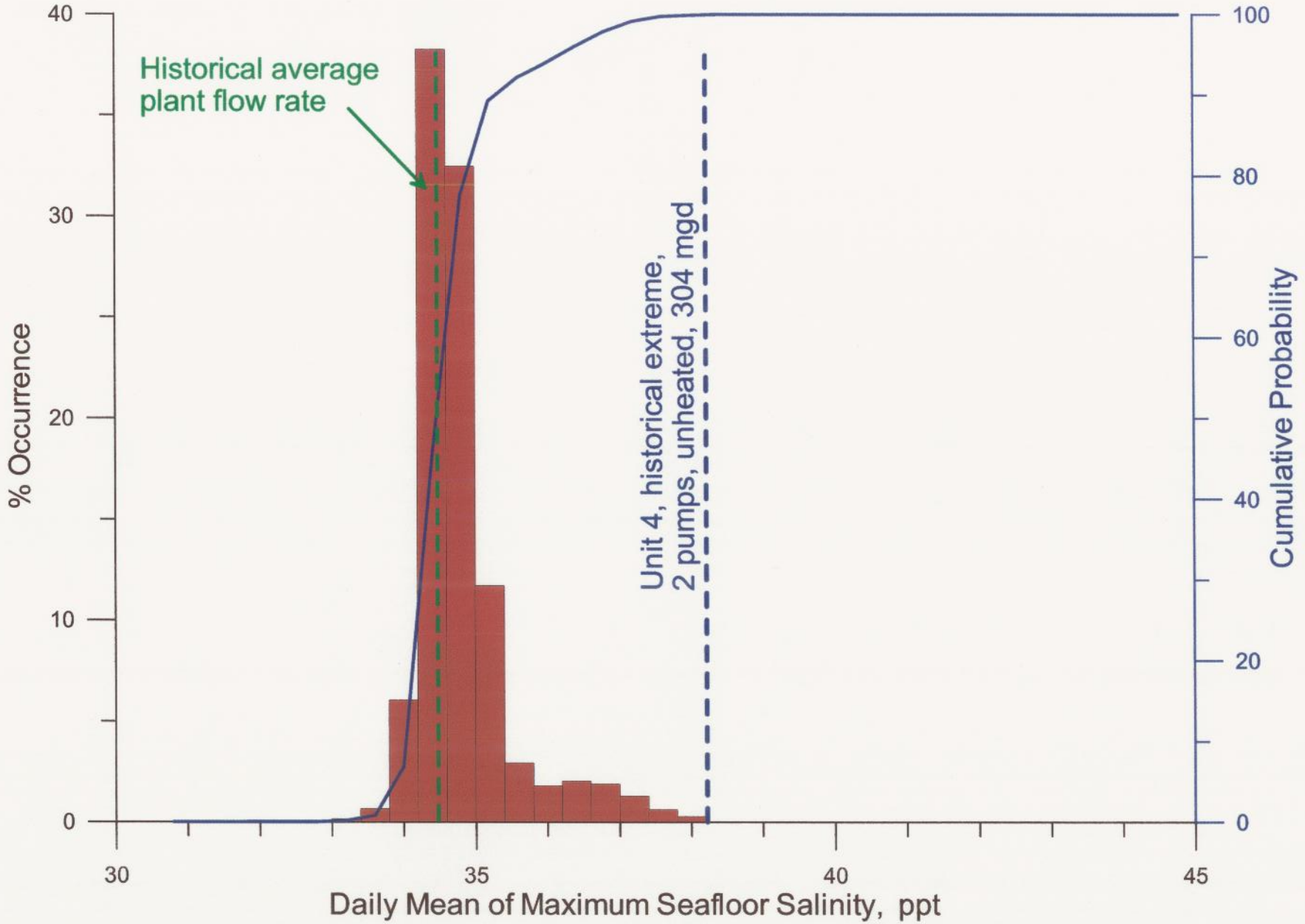

Figure E-2. Histogram of maximum seafloor salinity at 1000 ft from the discharge (outer edge of zone of initial dilution, ZID). Model results based on desalination at 50 mgd with a 40 ppt limit on end-of-pipe salinity applied to historic observations of Encina daily plant flow rates, ocean mixing, and water mass properties, 1980-2000. Vertical dashed lines give salinities at ZID for historical extreme model scenarios and average plant flow rate scenario.

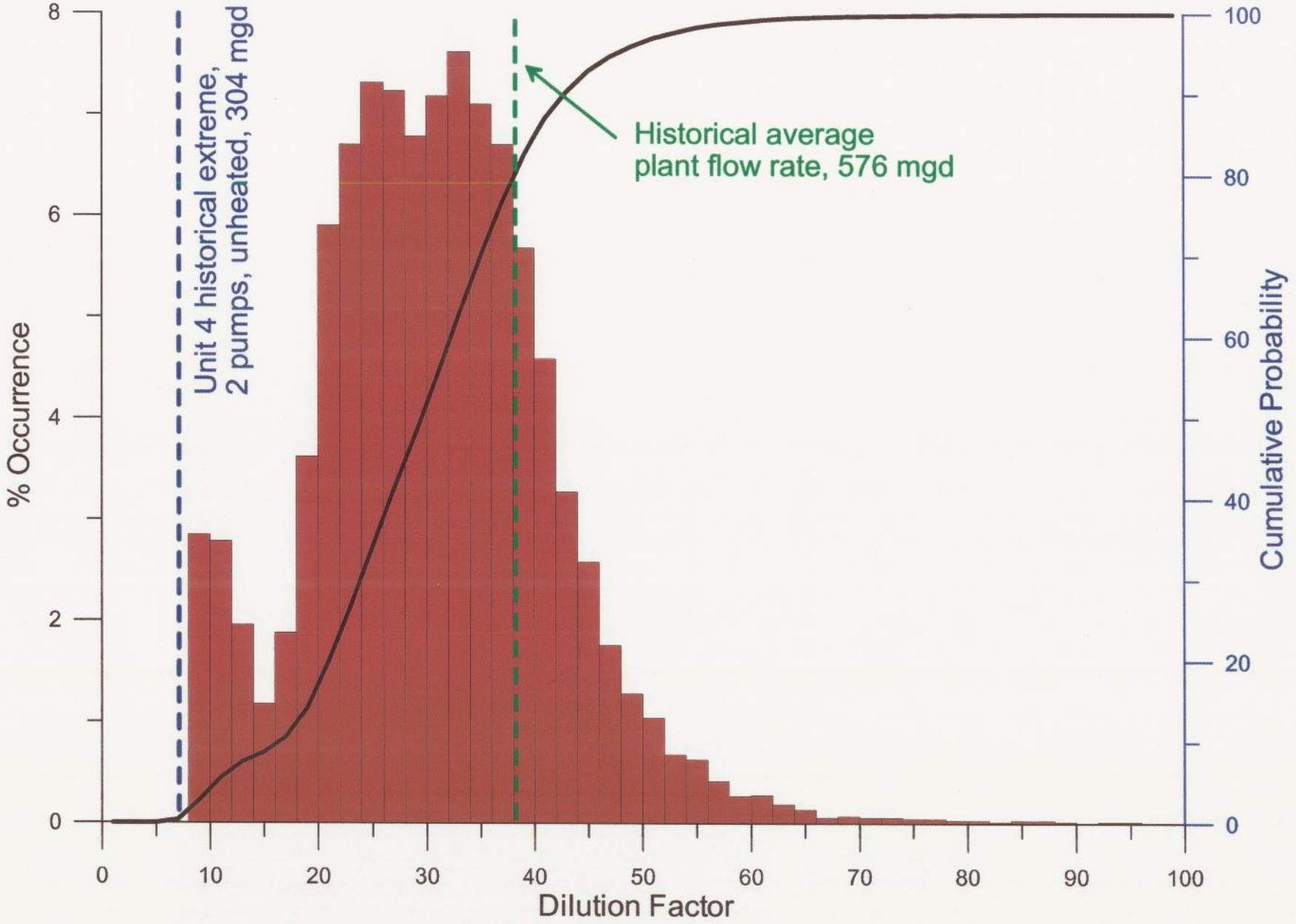

Figure E-3. Histogram of minimum dilution on the seafloor at 1000 ft from the discharge (outer edge of zone of initial dilution, ZID). Model results based on desalination at 50 mgd with a 40 ppt limit on end-of-pipe salinity applied to historic observations of Encina daily plant flow rates, ocean mixing, and water mass properties, 1980-2000. Vertical dashed lines give bottom dilution at ZID for historical extreme model scenarios and historical average plant flow rate.

Conclusions:

Based on these findings we conclude that the proposed Carlsbad Desalination Project when operated at a production level of 50 mgd and at power plant intake flow rates of 304 mgd or greater would produce a saline discharge that is everywhere less than 39 ppt, and thermal effects that are compliant with Water Quality Objectives under California's Thermal Plan. This suggests that a simple limit on end-of-pipe salinity at 40 ppt (as provided by a power plant intake flow rate limit of 304 mgd) would result in no significant impact in the receiving water.

1) Introduction

The proposed desalination plant will divert 100 mgd from the cooling water stream of the Encina power plant into a bank of high pressure reverse osmosis (RO) cartridges. The RO system will remove 50 mgd of fresh water from that diverted stream and return the remaining 50 mgd at twice ambient seawater salinity to the residual power plant cooling water stream. The primary concerns of this study are issues related to the discharge of concentrate from the desalination process into the receiving waters of the nearshore environment during the simultaneous occurrence of extreme case operating and environmental conditions. We will solve for temperature and salinity anomalies which these combined extreme circumstances cause in the marine environment.

The physical environment around the Encina Power Plant is quite dynamic due to an interplay between climatic variability and certain unique features of the physical setting. El Niño events cause significant warming and stratification of the coastal ocean around Encina over recurrence periods of 3 to 7 years. These warm El Niño events are superimposed on seasonal warming cycles. Tidal flow over the Carlsbad Canyon excites large amplitude internal waves at the same frequency of the tides (internal tides). These internal waves propagate on the temperature interface between the warm surface water (mixed layer) and the colder bottom water. Internal waves shoal and break in the shallow near shore waters just like the surface waves forming a kind of "internal surf" that runs up into the surfzone creating alternating episodes and patches of cold water that co-mingle with the warm surface water. Consequently, the baseline temperature fields of the

receiving waters around Encina have large temperature variations over time scales that fluctuate at periods of several years, seasonally, or daily.

The salinity field shows similar variability due to the same sets of climatic, seasonal, and tidal mechanisms. El Niño events bring floods causing river discharges of fresh water which depress the salinities of the coastal oceans in the vicinities of river mouths. Similar variations occur inter-annually as seasonal changes in wind patterns move different water masses with different salinities into and out of the Southern California Bight. The shoaling internal waves move higher salinity bottom water into the shallow nearshore and surfzone on hourly time scales. Therefore, the local environment already has a high degree of variability in temperature and salinity on which the activities of the power plant and desalination plants are superimposed. In addition the ocean forcing functions that will mix and carry away the heat and concentrated seawater resulting from these two activities are likewise modulated by El Niño events, seasonal changes in weather patterns and by diurnal and semi-diurnal changes in tidal stage. Even the power plant's production is effected by climatic, seasonal, and daily changes in user demand, with corresponding adjustments in the volume of lagoon water consumed by the plant and the amount of waste heat introduced into the coastal waters.

Altogether there are seven primary variables that enter into a solution for resolving the dispersion and dilution of the waste heat and concentrated seawater by-product of the combination of the power plant and desalination plant working in conjunction. These seven variables may be organized into ***boundary conditions*** and ***forcing functions***. The boundary conditions include: ocean salinity, ocean temperature, ocean water levels and power plant flow rates. There are two

additional boundary conditions which we will treat as constants: local bathymetry and power plant "Delta-T" (the amount that the power plant raises the cooling water above the ambient ocean temperature, where ambient ocean temperature is already treated as a variable). These boundary condition variables are developed in Section 3.1. The forcing function variables include: waves, currents, and winds are are developed in Section 3.2.

Overlapping 20.5 year long records containing 7,523 consecutive days between 1980 and 2000 are reconstructed in Sections 3.1 and 3.2 for each of the seven controlling variables. We search this 20.5 year period for the historical combination of these variables that give an historic extreme day in the sense of benign ocean conditions that minimize mixing and dilution rates, and an average day giving typical mixing and dilution rates. We then overlay our historical extreme scenarios on those environmental conditions. The criteria for a historical extreme day was based on the simultaneous occurrence of the environmental variables having the highest combination of absolute salinity and temperature during the periods of lowest mixing and advection in the local ocean environment. In the historical extreme day scenarios low mixing and dilution periods coincide with periods of minimal wave, wind, currents, and ocean water levels (including both tidal oscillations and climatic variability that causes sea level anomalies). The average day scenarios were found by a statistical search of these records for the average 24 hour combinations of the 7 variables occurring over the 20.5 year period of record. This procedure produced the model scenarios defined in Section 3.3. We also set up the model in Section 3.3 to solve for the properties of the saline plume for all 7523 combinations of the 7 controlling variables in order to establish

the statistical likelihood of the historical extreme scenarios. To provide a manageable set of outcomes, these 20.5 year-long simulations solved for the depth averaged and bottom salinities and dilutions at the edge of the ***zone of initial dilution*** (or ***ZID***, a semi-circle with a 1000 foot radius around the discharge channel).

The technical approach used to evaluate these scenarios for historical extremes and average case conditions involved the use of hydrodynamic transport models detailed in the Part 1 study of Jenkins and Wasyl (2001). It is described briefly in Section 2 and calibrated in Section 3.4. The dispersion and dilution of concentrated seawater produced by the proposed desalination plant was evaluated for 4 separate historical extreme scenarios in Sections 4.1 through 4.4. These are contrasted with the average case scenario in Section 4.5 and long term simulations of the entire 20.5 year period of record in Section 4.6. Summary tables of the results and conclusions are presented in Section 5.

2) Model Description and Capabilities

This study utilizes a coupled set of numerical tidal and wave transport models to evaluate dilution and dispersion when the proposed desalination plant is producing 50 mgd of product water while the power plant is operated in a variety of historical extreme cases. The numerical model used to simulate tidal currents in the nearshore and shelf region of Encina is the finite element model **TIDE_FEM**. Wave-driven currents are computed from the shoaling wave field by a separate model, **OCEANRDS**. The dispersion and transport of concentrated seawater and storm water discharge by the wave and tidal currents is calculated by the finite element model known as **SEDXPORT**.

The finite element research model, **TIDE_FEM**, (Jenkins and Wasyl, 1990; Inman and Jenkins, 1996) was employed to evaluate the tidal currents inside Agua Hedionda Lagoon and along a nearshore region extending between Oceanside and Encinitas, CA. **TIDE_FEM** was built from some well-studied and proven computational methods and numerical architecture that have done well in predicting shallow water tidal propagation in Massachusetts Bay (Connor and Wang, 1974) and along the coast of Rhode Island, (Wang, 1975), and have been reviewed in basic text books (Weiyan, 1992) and symposia on the subject, e.g., Gallagher (1981). The governing equations and a copy of the core portion of the **TIDE_FEM** FORTRAN code are found in Appendix B of the Part 1 study of Jenkins and Wasyl, (2001). **TIDE_FEM** employs a variant of the vertically integrated equations for shallow water tidal propagation after Connor and Wang (1975). These are based upon the Boussinesq approximations with Chezy friction

and Manning's roughness. The finite element discretization is based upon the commonly used **Galerkin weighted residual method** to specify integral functionals that are minimized in each finite element domain using a variational scheme, see Gallagher (1981). Time integration is based upon the simple **trapezoidal rule** (Gallagher, 1981).

The computational architecture of **TIDE_FEM** is adapted from Wang (1975), whereby a transformation from a **global** coordinate system to a **natural** coordinate system based on the unit triangle is used to reduce the weighted residuals to a set of order-one ordinary differential equations with constant coefficients. These coefficients (**influence coefficients**) are posed in terms of a **shape function** derived from the natural coordinates of each nodal point in the computational grid. The resulting systems of equations are assembled and coded as banded matrices and subsequently solved by **Cholesky's method**, see Oden and Oliveira (1973) and Boas (1966). The hydrodynamic forcing used by **TIDE_FEM** is based upon inputs of the tidal constituents derived from Fourier decomposition of tide gage records. Tidal constituents are input into the module **TID_DAYS**, which resides in the hydrodynamic forcing function cluster (see Appendix C of the Part 1 study of Jenkins and Wasyl, 2001, for a listing of TID_DAYS code). **TID_DAYS** computes the distribution of sea surface elevation variations in the ocean off Encina and adjacent nearshore after compensating for phase shifts associated with travel time between the Scripps Pier tide gage station (NOAA #941-0230) and Encina. Forcing for **TIDE_FEM** is applied by the distribution in sea surface elevation across the deep water boundary of the computational domain. Here the tidal currents reduce to the deep water solutions to Laplace's tidal

equations (Lamb, 1932). The x-component (longitudinal) of the deep water tidal current is given by:

$$u_{x,\infty} = \frac{ig}{a}\left[\frac{2\Omega s\cot\theta(\xi-\bar{\xi})+\varpi\left(\frac{d\xi}{d\theta}-\frac{d\bar{\xi}}{d\theta}\right)}{\varpi^2-(2\Omega\cos\theta)^2}\right] \quad (1)$$

while the y-component (latitudinal) is:

$$u_{y,\infty} = \frac{g}{a}\left[\frac{s\varpi\csc\theta(\xi-\bar{\xi})\Omega\cos\theta\left(\frac{d\xi}{d\theta}-\frac{d\bar{\xi}}{d\theta}\right)}{\varpi^2-(2\Omega\cos\theta)^2}\right] \quad (2)$$

where θ is the co-latitude; $\bar{\xi}$ is the equilibrium tide; g is the acceleration of gravity; Ω is the angular speed of rotation of the earth, a is the mean radius of the earth; s is an integer; ϖ is the radian frequency of the potential tide as determined from the tidal constituents.

Wave driven currents were calculated from wave measurements by Scripps SAS station at Torrey Pines (Pawka, 1982) and by the CDIP arrays at Huntington Beach, San Clemente, and Oceanside, CA, see CDIP (2000). These measurements were back refracted out to deep water to correct for island sheltering effects between the monitoring sites and the Encina/Carlsbad region. The waves were then forward refracted onshore to give the variation in wave heights, wave lengths and directions throughout the nearshore around Encina. The numerical refraction-diffraction code used for both the back refraction from these wave monitoring sites

out to deep water, and the forward refraction to the Encina Power Plant site is **OCEANRDS** and may be found in Appendix D of the Part 1 study of Jenkins and Wasyl, (2001). This code calculates the simultaneous refraction and diffraction patterns of the swell and wind wave components propagating over bathymetry replicated by the **OCEANBAT-f** code. **OCEANBAT-f** generates the associated depth fields for the computational grid networks of both **TID_FEM** and **OCEANRDS** using packed bathymetry data files derived from the National Ocean Survey (NOS) depth soundings. The structured depth files written by **OCEANBAT-f** are then throughput to the module **OCEANRDS-f**, which performs a refraction-diffraction analysis from deep water wave statistics. **OCEANRDS-f** computes local wave heights, wave numbers, and directions for the swell component of a two-component, rectangular spectrum. These values are then throughput to **WINDWAVE-f**, which completes the refraction-diffraction analysis of the two-component spectrum including wind wave effects up to Nyquist frequencies.

The wave data are throughput to a wave current algorithm in **SEDXPORT** which calculates the wave-driven longshore currents, v(r). These currents were linearly superimposed on the tidal current. The wave-driven longshore velocity, v(r), is determined from the longshore current theories of Longuet-Higgins (1970), according to:

$$\bar{v}(r) = v_o \left(\frac{10}{49} \frac{r}{X_b} - \frac{5}{7} \ln \frac{r}{X_b} \right) \text{ if } 0 \le r \le X_b$$

$$= v_o \frac{10}{49} \left(\frac{r}{X_b} \right)^{5/2} \text{ if } r > X_b \qquad (3)$$

$$v_o = \frac{5\pi}{8} \frac{0.41}{C_D} (g h_b)^{1/2} \beta \sin\alpha_b$$

where r is the shoreline-normal coordinate, X_b is the width of the surf zone, taken as $X_b \equiv 5/4\ H_b \tan\beta$, H_b is the breaker height from the refraction solution, $\tan\beta$ is the beach slope, α_b is the breaker angle, h_b is the breaker depth, taken as $h_b = 5/4 H_b$. C_D is the drag coefficient, and g is the acceleration of gravity. Inspection of (3) reveals that the longshore transport is strongest in the neighborhood of the breakpoint, $r = X_b$, where the longshore currents approach a maximum value of $v(r) = v_o$.

Once the tidal and wave driven currents are resolved by **TIDE_FEM and OCEANRDS** and **WINDWAVE**, the dilution and dispersion of flood water runoff and concentrated seawater discharge in those flows is computed by the stratified transport model **SEDXPORT** . The **SEDXPORT** code is a time stepped finite element model which solves the advection-diffusion equations over a fully configurable 3-dimensional grid. The vertical dimension is treated as a two-layer ocean, with a surface mixed layer and a bottom layer separated by a pycnocline

interface. The code accepts any arbitrary density and velocity contrast between the mixed layer and bottom layer that satisfies the Richardson number stability criteria and composite Froude number condition of hydraulic state.

The combined discharge of the power plant and desalination plant is represented as sources in the surface mixed layer. The Encina infall is similarly treated as a sink. The source initializations for the plant infall and outfall are handled by a companion code called **MULTINODE** that couples the computational nodes of **TIDE_FEM** and **OCEANRDS** with **SEDXPORT**. The codes do not time split advection and diffusion calculations, and will compute additional advective field effects arising from spatial gradients in eddy diffusivity, i.e., the so-called "gradient eddy diffusivity velocities" after Armi (1979). Eddy mass diffusivities are calculated from momentum diffusivities by means of a series of Peclet number corrections based upon TSS and TDS mass and upon the mixing source. Peclet number corrections for the surface and bottom boundary layers are derived from the work of Stommel (1949) with modifications after Nielsen (1979), Jensen and Carlson (1976), and Jenkins and Wasyl (1990). Peclet number correction for the wind-induced mixed layer diffusivities are calculated from algorithms developed by Martin and Meiburg (1994), while Peclet number corrections to the interfacial shear at the pycnocline are derived from Lazara and Lasheras (1992a;1992b). The momentum diffusivities to which these Peclet number corrections are applied are due to Thorade (1914), Schmidt (1917), Durst (1924), and Newman (1952) for the wind-induced mixed layer turbulence and to Stommel (1949) and List, et al. (1990) for the current-induced turbulence. The primitive equations for the **SEDXPORT** code may be found in Appendix E of the

Part 1 study of Jenkins and Wasyl, (2001), and in Appendix F of the same report for **MULTINODE**.

In it's most recent version, **SEDXPORT** has been integrated into the Navy's Coastal Water Clarity Model and the Littoral Remote Sensing Simulator (LRSS) (see Hammond, et al., 1995). The **SEDXPORT** code has been validated in mid-to-inner shelf waters (see Hammond, et al., 1995; Schoonmaker, et al., 1994). Validation of the SEDXPORT code was shown by three independent methods: 1) direct measurement of suspended particle transport and particle size distributions by means of a laser particle sizer; 2) measurements of water column optical properties; and, 3) comparison of computed stratified plume dispersion patterns with LANDSAT imagery.

Besides being validated in coastal waters of Southern California, the **SEDXPORT** modeling system has been extensively peer reviewed. Although some of the early peer review was confidential and occurred inside the Office of Naval Research and the Naval Research Laboratory, the following is a listing of 5 independent peer review episodes of SEDXPORT that were conducted by 8 independent experts and can be found in the public records of the State Water Resources Control Board, the California Coastal Commission and the City of Huntington Beach.

1997- Reviewing Agency: State Water Resources Control Board

Project: NPDES 316 a/b Permit renewal, Encina Power Plant, Carlsbad, CA

Reviewer: Dr. Andrew Lissner, SAIC, La Jolla, CA

1998- Reviewing Agency: California Coastal Commission

Project: Coastal Development Permit, San Dieguito Lagoon Restoration

Reviewers: Prof. Ashish Mehta, University of Florida, Gainesville
Prof. Paul Komar, Oregon State University, Corvallis
Prof. Peter Goodwin, University of Idaho, Moscow

2000- Reviewing Agency: California Coastal Commission

Project: Coastal Development Permit, Crystal Cove Development

Reviewers: Prof. Robert Wiegel, University of California, Berkeley
Dr. Ron Noble, Noble Engineers, Irvine, CA

2002- Reviewing Agency: California Coastal Commission

Project: Coastal Development Permit, Dana Point Headland Reserve

Reviewers: Prof. Robert Wiegel, University of California, Berkeley
Dr. Richard Seymour, University of California, San Diego

2003- Reviewing Agency: City of Huntington Beach

Project: EIR Certification, Poseidon Desalination Project

Reviewer: Prof. Stanley Grant, University of California, Irvine

SEDXPORT has been built in a modular computational architecture with a set of subroutines divided into two major clusters: 1) those which prescribe hydrodynamic forcing functions; and, 2) those which prescribe the mass sources

acted upon by the hydrodynamic forcing to produce dispersion and transport. The cluster of modules for hydrodynamic forcing ultimately prescribes the velocities and diffusivities induced by wind, waves, and tidal flow for each depth increment at each node in the grid network. The subroutines **RIVXPORT** and **BOTXPORT-f** in **SEDXPORT-f** solve for the mixing and advection of the negatively buoyant concentrated seawater in response to the wave and tidal flow using an rms vorticity-based time splitting scheme. Both **BOTXPORT** and **RIVXPORT** solve the eddy gradient form of the advection diffusion equation for the water column density field

$$\frac{\partial \rho}{\partial t} = (u - \nabla \epsilon) \bullet \nabla \rho - \epsilon \nabla^2 \rho \qquad (4)$$

where u is the vector velocity from a linear combination of the wave and tidal currents, ε is the mass diffusivity and ρ is the water mass density. The primitive equations for the heat transport in SEDXPORT have the form:

$$\frac{\partial Q}{\partial t} = (u - \nabla \epsilon_H) \cdot \nabla Q - \epsilon_H \nabla^2 Q + Q_o V(t)$$
$$dQ = C_p dT \qquad (5)$$

where dQ is the increment of heat per unit mass due to a temperature differential, dT; Q_o is the heat per unit mass initially imparted to the cooling water as it leaves the plant due to a temperature differential ΔT between the plant intake and outfall temperatures; $V_o(t)$ is the non-dimensional plant flow rate normalized by the tidal

prism; C_p is the heat capacity of seawater at constant pressure, ϵ_H is the diffusivity of heat, u is the vector resultant of the longshore velocity, $\bar{v}(x)$, the tidal current, u_n, and the discharge velocity $u_o(t)$; and ∇ is the vector gradient operator. In Equations (4 and 5) the last term is the heat source term and the term $-\nabla\epsilon_H$ acts much like an additional advective field in the direction of high to low eddy diffusivity. This additional "gradient eddy diffusivity velocity" is the result of local variations in wave intensity associated with the refraction/diffraction pattern, and is strongest in the wave shoaling region nearshore. For further details see Appendix E of the Part 1 study of Jenkins and Wasyl, (2001).

The water mass density is a function of temperature, *T*, and salinity, *S*, according to the equation of state expressed in terms of the specific volume, $\alpha = 1/\rho$, or:

$$\frac{d\alpha}{\alpha} = \frac{1}{\alpha}\frac{\partial\alpha}{\partial T}dT + \frac{1}{\alpha}\frac{\partial\alpha}{\partial S}dS \qquad (6)$$

The factor $\partial\alpha/\partial T$, which multiplies the differential temperature changes, is known as the coefficient of thermal expansion and is typically 2×10^{-4} per °C for seawater; the factor $\partial\alpha/\partial S$ multiplying the differential salinity changes, is the coefficient of saline contraction and is typically 8×10^{-4} per part per thousand (ppt) where 1.0 ppt = 1.0 g/L of total dissolved solids (TDS). For a standard seawater, the specific volume has a value $\alpha = 0.97264$ cm^3/g. If the percent change in specific volume by equation (6) is less than zero, then the new water mass is heavier than standard seawater, and lighter if the percent change is greater than zero. Solutions to the

density field calculated from equation (4) by **SEDXPORT** are used to calculate the field salinity, $S_{(x, y, z)}$, from equation (6) for temperature inputs T for the ambient ocean water and ΔT for plant thermal effluent. The salinity field in turn can be used to solve for the spacial varying dilution factor, $D_{(x, y, z)}$ according to:

$$D_{(x,y,z)} = \frac{S_b - S_o}{S_{(x,y,z)} - S_o} \tag{7}$$

where S_o is the ambient seawater salinity in ppt, S_b is the end-of-the-pipe salinity of concentrated seawater and $S_{(x, y, z)}$ is the local salinity from the model solution in ppt. Model solutions will find a significant variation in the salinity with water depth, z. Therefore we introduced a depth averaged dilution factor,

$$\bar{D}_{(x,y,z)} = \frac{1}{H_{(x,y)}} \int_0^H D_{(x,y,z)}\, dZ \tag{8}$$

where $H = H_{(x, y)} = h + \eta$ is the local water depth, h is the local water depth below mean sea level and η is the tidal amplitude.

The diffusivity, ε, in equations (4 and 5) controls the strength of mixing and dilution of the concentrated seawater and flood water constituents, and varies with position in the water column relative to the pycnocline interface. Vertical mixing includes two mixing mechanisms at depths above and below the pycnocline: 1) fossil turbulence from the bottom boundary layer, and 2) wind mixing in the surface mixed layer. The pycnocline depth is treated as a zone of hindered mixing and

varies in response to the wind speed and duration. Below the pycnocline, only turbulence from the bottom wave/current boundary layer contributes to the local diffusivity. Nearshore, breaking wave activity also contributes to mixing. The surf zone is treated as a line source of turbulent kinetic energy by the subroutine **SURXPORT-f**. This subroutine calculates seaward mixing from fossil surf zone turbulence, and seaward advection from rip currents embedded in the line source. Both the eddy diffusivity of the line source and the strength and position of the embedded rip currents are computed from the shoaling wave parameters evaluated at the breakpoint, as throughput of **OCEANRDS-f**.

3) Model Initialization

Uninterrupted, long-term monitoring of ocean properties has not been maintained at Encina, but has been at the nearby Scripps Pier. The Scripps Pier site has many physical features in common with the nearshore area around Encina. Both sites have a narrow shelf and a submarine canyon nearby. Consequently internal waves are an active mechanism at both sites in causing daily (diurnal) variations in salinity, temperature, and other ocean properties. The longer period variations at seasonal and multiple year time scales are the same at both sites due to their proximity. Consequently the Scripps Pier Shore Station data (SIO, 2001) and the Coastal Data Information Program monitoring at Scripps Pier (CDIP, 2001) are used as surrogates for long term records of physical ocean properties at Encina. These properties will be shown to exhibit considerable natural variability over the period of record from 1980 to mid 2000 due to daily and seasonal changes, but most especially due to climate changes, (see the Part 1 study of Jenkins and Wasyl, 2001, for more detail on climate cycles).

3.1) Boundary Conditions

A) Power Plant Flow Rates: The power plant cooling water is drawn from the lagoon and is discharged into the ocean through an independent discharge channel located between Middle Beach and South Beach. Plant flow rate data was provided in hourly increments on an ASCII-formatted diskette by the power plant owner/operator, Cabrillo Power I LLC. A histogram of the plant flow rates for 1999 was constructed and compared against the flow rate histogram for 1993-94 from Jenkins & Wasyl (1994). Although flow rates above 70% capacity were more

common in 1999 than 1994, the mean flow rate is relatively unchanged. This is due to the fact that the plant operates pumps according to a number of operational requirements of the western power grid that often reflect factors other than local user demand for electrical power. Because of the apparent minor differences in annual flow volume from year to year, the 1999 flow rate history will be utilized as a surrogate for all years in the model problem. This was done to project contemporary user demand on all historical extreme scenarios. The resulting 20.5 year long time series for project flow rate obtained by looping the 1999 year record is shown in Panel-a of Figure 1. Inspection of Figure 1a indicates that flow rates of 735-800 mgd are fairly representative of the high user demand during warm weather. The average rate of cooling water flow was 550 mgd which is very close to a rate of utilization at 70% of maximum capacity (570 mgd), where maximum capacity is 808 mgd. No flow rates less than 200 mgd were recorded.

B) Ocean Salinity: Since the discharge channel at Encina discharges into the surfzone, the surface salinity monitoring data from Scripps Pier was used for reconstruction of a 20.5 year record of ocean salinity in the nearshore of Encina, as shown in Panel-b of Figure 1. In the period of record from 1980 through mid 2000, the maximum recorded salinity was 34.44 ppt (parts per thousand) and the minimum was 31.26 ppt. Smaller variations occurred over daily and seasonal time scales, while the maximum range of salinity variation (10%) was concurrent with the powerful 1993 (ENSO cycle). The 20.5 year average salinity was 33.52 ppt.

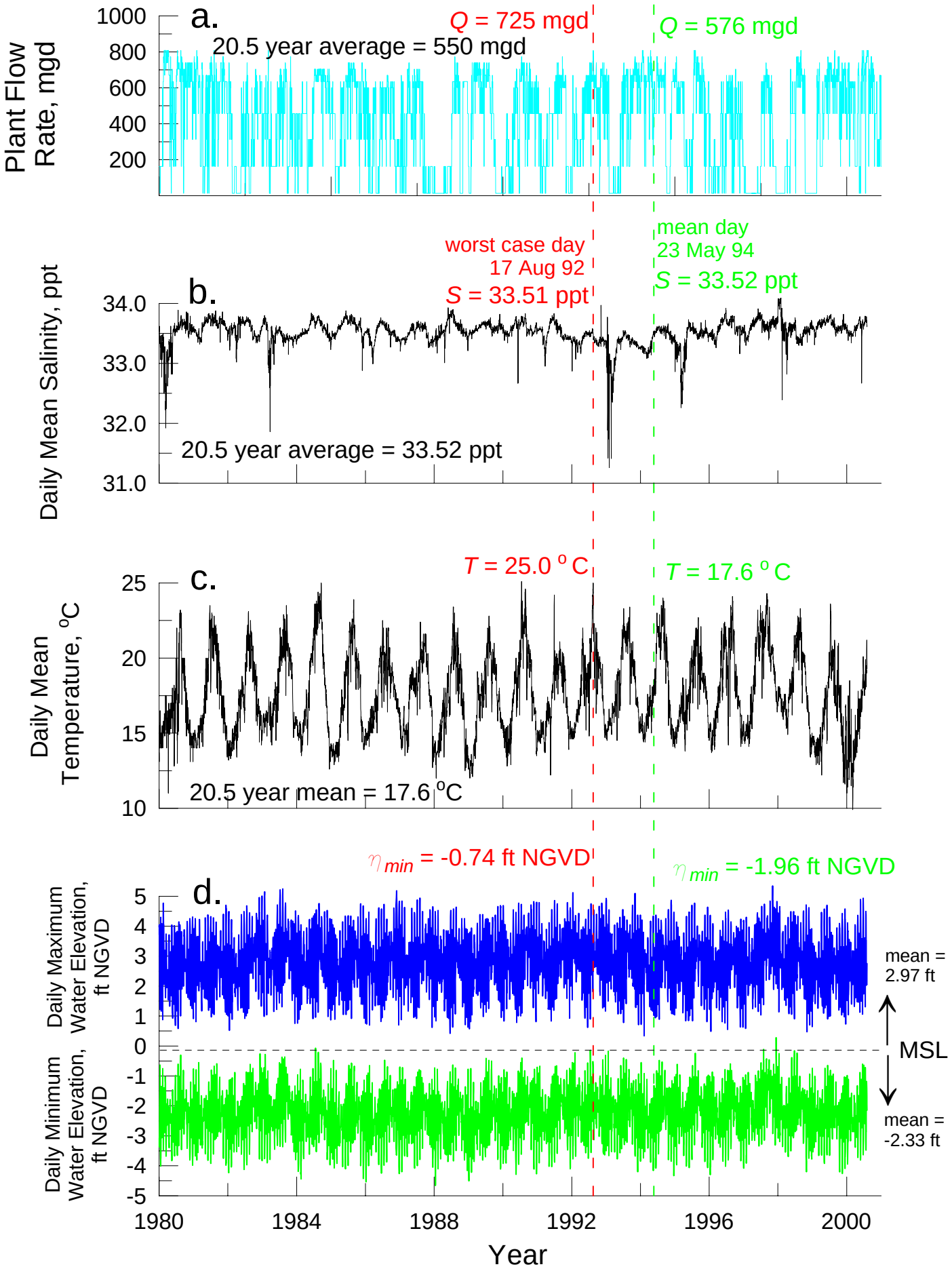

Figure 1. Period of record of boundary conditions, Encina Power Plant, 1980-2000.5: a) plant flow rate b) daily mean salinity, c) daily mean temperature, and d) daily high and low water elevations.

C) Ocean Temperature: Because the Encina Power Plant discharges into the surfzone, we use ocean surface temperature off Scripps Pier to characterize the temperature environment off Encina. The 20.5 year long reconstruction of surface temperatures from the Scripps Pier Shore Station monitoring is given in Panel-c of Figure 1. A pronounced seasonal variation in these temperatures is quite evident with the maximum recorded daily mean temperature reaching 25.1 °C during the summer of the 1993 El Niño and the minimum falling to 9.9 °C during the winter of the 1999-2000 La Niña. The 20.5 year mean temperature was found to be 17.6 °C. Consequently natural temperature variability of the coastal waters in the vicinity of the Scripps Pier and Encina Power Plant is on the order of 86%.

D) Ocean Water Levels: Dilution levels in the discharge channel is limited by the time variation in ocean water level, and by the rate of cooling water consumption by the Encina power plant. The ocean water level is monitored by tide gages. The nearest ocean tide gage station that measures ocean water levels near Encina is located at Scripps Pier, La Jolla, CA. This tide gage (NOAA #941-0230) was last leveled using the 1960-78 tidal epoch, which resulted in the following tidal datum:

MEAN HIGHER HIGH WATER (MHHW) = +2.81 FT. NGVD

MEAN HIGH TIDE (MHT) = +2.06 FT. NGVD

MEAN SEA LEVEL (MSL) = +0.19 FT. NGVD

MEAN LOWER LOW WATER (MLLW) = -2.56 FT. NGVD

Water levels measured by the Scripps Pier Tide Gage (#941-0230) have been archived by NOAA (2000) for the preceding 20.5 year period, 1980 through mid

2000. Reconstruction of a water level time series was performed on the entire set of 1980-2000 NOAA measurements. The resulting time series of daily maximum and minimum ocean water levels is plotted in Panel-d of Figure 1. The phenomena of positive sea level anomalies is a persistent and sustained occurrence in the observations of ocean water levels during the last 20 years. A very significant number of diurnal tide cycles during the last 20 years (466) have produced water level elevations well in excess of the extreme higher-high water levels (EHHW) of the astronomic tides, where EHHW = +4.28 ft. NGVD for a perigean spring tide occurring once every 4.5 years. The occurrence of extreme water levels in excess of the astronomic tides are not merely rare, isolated events. In the period of record shown by the blue trace in Figure 1d, the maximum ocean water level was +5.35 ft. NGVD occurring during the 1997 El Niño, 1.31 ft. higher than the astronomic tides of the tide tables. These high water levels promote additional initial dilution of the concentrated sea salts from desalination because they provide additional dilution volume in the discharge channel. On the other hand, the minimum ocean water level was -4.66 ft. NGVD, occurring during the 1988 winter. These low water levels shown in the green trace of Figure 1d reduce initial dilution of the concentrated sea salts.

E) Power Plant Operating Temperatures: Section 316(a) of the Clean Water Act requires compliance with the State water quality standards for the discharge of thermal effluent. The State of California Regional Water Resources Control Board accepted delegation of the National Pollutant Elimination System permit program from the U.S. Environmental Protection Agency in 1972.

California's Thermal Plan incorporates provisions of Section 316(a) of the Federal Water Pollution Control Act of 1972 and defines the relevant regulatory requirements for cooling water discharge from the Encina Power Plant. The applicable regulatory requirements are found in those sections of the Thermal Plan dealing with Specific Water Quality Objectives, General Water Quality Provisions, and provisions within the implementation section. As an existing discharge to coastal waters, Encina Units 1 through 5 have the following Specific Water Quality Objectives:

- 3A(1) - Elevated temperature wastes shall comply with limitations necessary to assure protection of beneficial uses and areas of special biological significance.

- 3B(1) - Elevated temperature wastes shall be discharged to the open water away from the shoreline to achieve dispersion through the vertical water column.

- 3B(2) - Elevated temperature wastes shall be discharged a sufficient distance from areas of special biological significance to assure the maintenance of natural temperature in these areas.

- 3B(3) - The maximum temperature of thermal waste discharges shall not exceed the natural temperature of receiving waters by more than 20 °F.

•3B(4) - The discharge of elevated temperature wastes should not result in increases in the natural water temperature exceeding 4 °F at the: (a) shoreline, (b) surface of any ocean substrate, or c) ocean surface beyond 305 m (1000 ft) from the discharge system. The surface temperature limitation shall be maintained at least 50% of the duration of any complete tidal cycle.

The last of these objectives, item c of 3B(4), defines the boundary on the zone of initial dilution (ZID).

In 1999 the operation of Encina Power Plant was taken over from San Diego Gas and Electric Company by NRG Cabrillo Power Operations, Inc. Although certified to discharge thermal waste at as much as 20 °F (11 °C) above ambient ocean temperatures, (Delta-T = ΔT = 20 °F = 11 °C), the new plant operators have adopted operating procedures that discharge considerably below the maximum certified Delta-T. Panel-a in Figure 2 plots the intake and discharge temperature history under the new plant operating procedures for a period concurrent with the last half of the plant flow rate history shown in Figure 1a. The discharge temperatures occasionally spike to as high as 45 °C during short term heat treatment cycles performed to remove bio-fouling from the cooling water circulation system. Otherwise the plant discharge temperatures track the ambient ocean temperatures rather clearly with an average Delta-T of ΔT = 5.5 °C (see

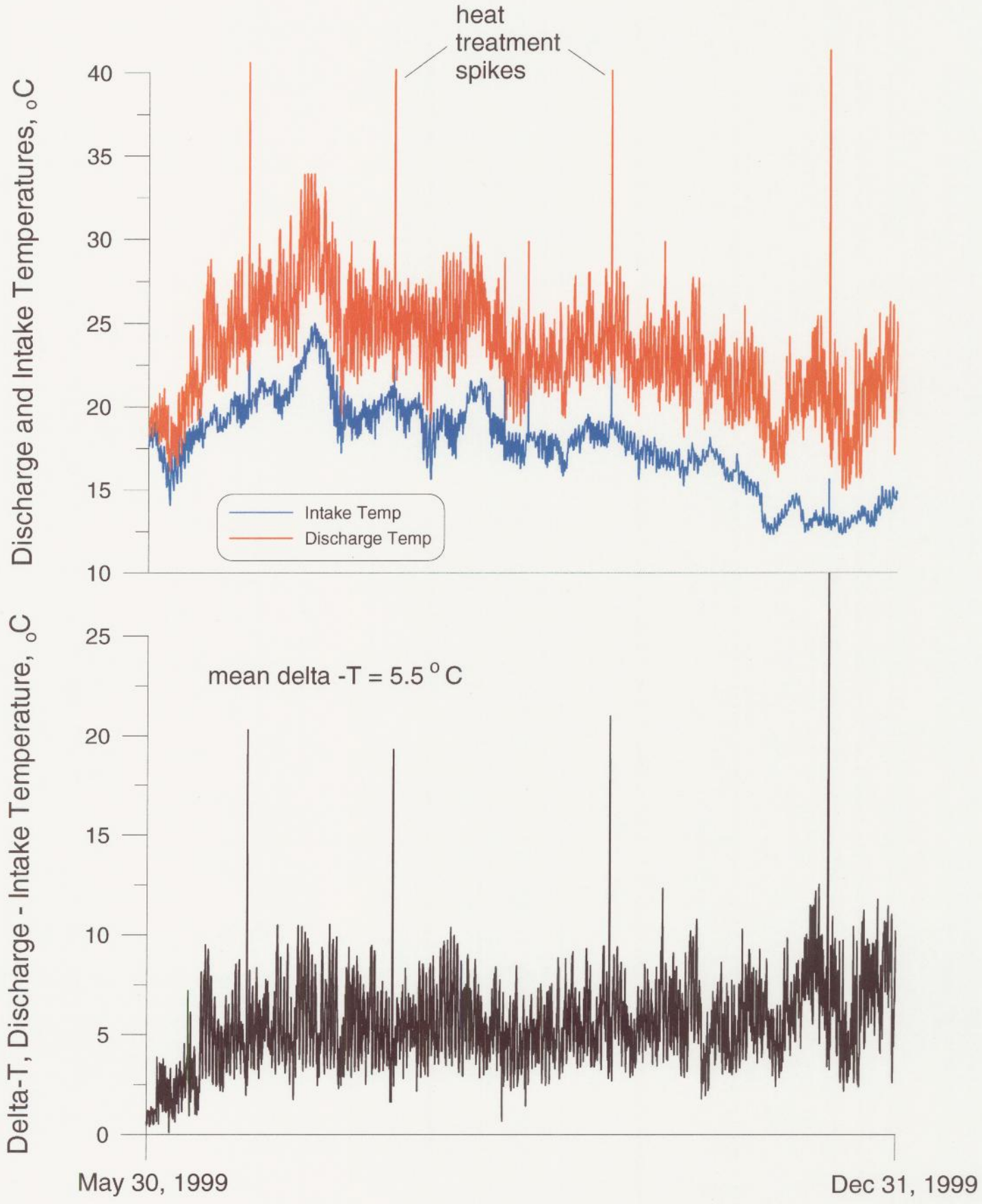

Figure 2 . Operating temperatures, Encina Power Plant, a) Intake and discharge temperatures; b) Delta-T

Panel-b of Figure 2). This value is used for "heated" model scenarios performed in this study. For the "unheated" scenarios, the Delta-T was set at $\Delta T = 0$ °C

F) Bathymetry: Bathymetry provides a controlling influence on all of the coastal processes at work in both the nearfield and farfield of Encina. The bathymetry consists of two parts: 1) a stationary component in the offshore where depths are roughly invariant over time, and 2) a non-stationary component in the nearshore where depth variations do occur over time. The stationary bathymetry generally prevails at depths that exceed ***closure depth*** which is the depth at which net on/offshore transport vanishes. Closure depth is typically -15 m MSL in the Oceanside Littoral Cell, [Inman et al. 1993]. The stationary bathymetry was derived from the National Ocean Survey (NOS) digital database as plotted in Figure 3 seaward of the 15m depth contour. Gridding is by latitude and longitude with a 3 x 3 arc second grid cell resolution yielding a computational domain of 15.4 km x 18.5 km. Grid cell dimensions along the x-axis (longitude) are 77.2 meters and 92.6 meters along the y-axis (latitude). This small amount of grid distortion is converted internally to Cartesian coordinates, using a Mercator projection of the latitude-longitude grid centered on Agua Hedionda Lagoon. The convention for Cartesian coordinates uses x-grid spacings for longitude and y-grid spacings for latitude. Any depths below 305 meters are assigned default values of 305 m. while any land masses or shoals above 0-MSL are assigned default values of -1.14 m.

For the non-stationary bathymetry data inshore of closure depth (less than -15 m MSL) a precision GPS nearshore and beach survey was conducted in September 2000 [Dyson, 2000]. These nearshore and beach survey data are

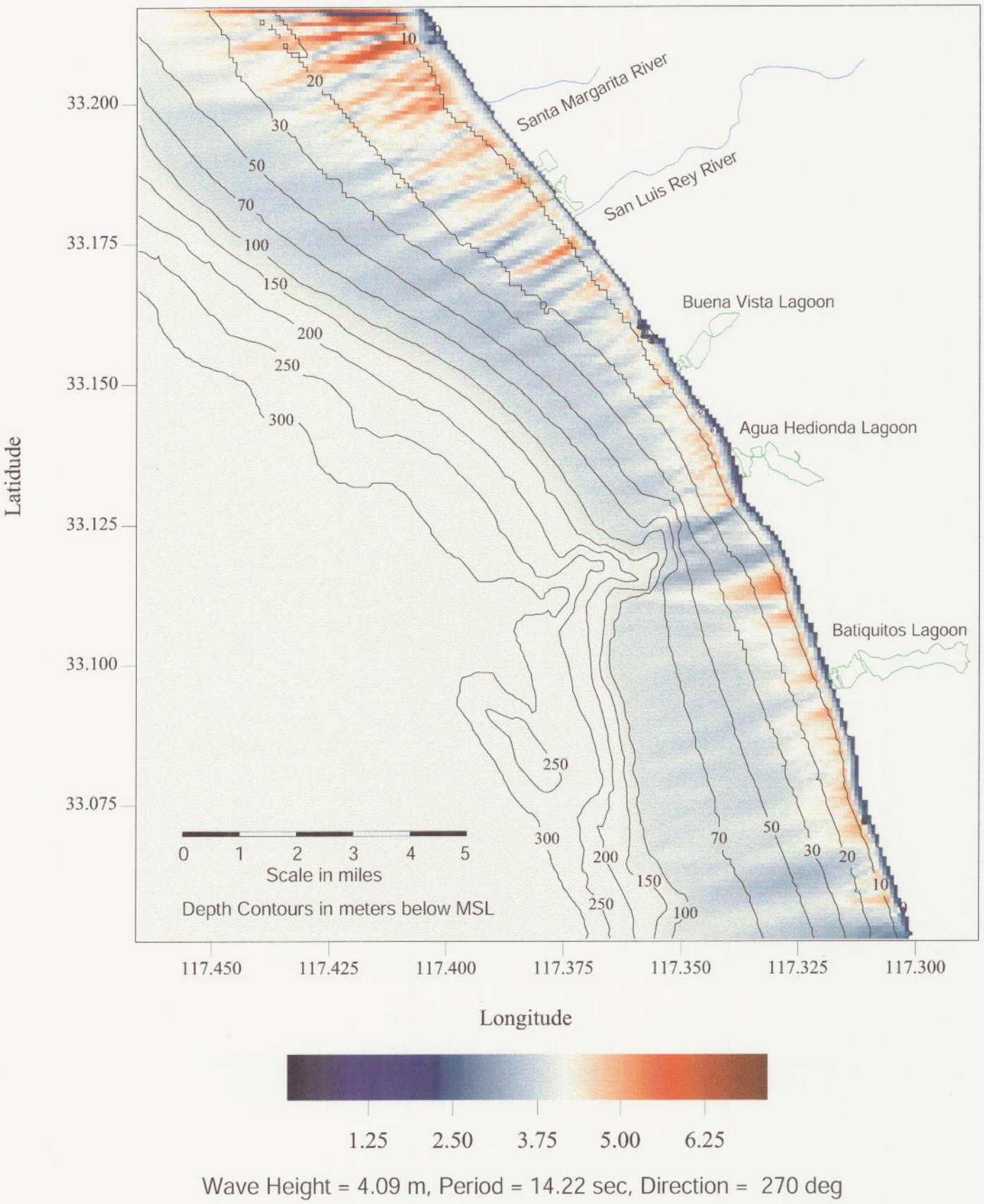

Figure 3. Maximum Event Wave Refraction for Period of Record 1980-2000 (18 January 1988)

plotted in Figure 3 landward of the 15m depth contour. The September 2000 nearshore bathymetry database was merged with the NOS database to generate the bathymetry for both the farfield computational domain in Figure 3 and the nearfield computational domain shown in Figures 7 through 23.

3.2) Forcing Functions

A) Waves: Because the combined discharge of the power plant and desalination plant are discharged into the surfzone, the wave climate exerts leading order control on the initial dilution and dispersion of both the waste heat and the concentrated seawater by-product from RO production. The wave climate at Encina is strongly modulated by seasonal storms and by the ENSO and PNA induced climatic variations described in Section 3.1 of the Part 1 study of Jenkins and Wasyl, (2001). Wave data is also the limiting data base among the 7 controlling variables. The 1980-July period of record used in this study was constrained by the longest period for which continuous unbroken records of wave height, period and direction could be obtained.

Waves have been routinely monitored at several locations in the lower Southern California Bight since 1980 by the Coastal Data Information Program, [CDIP, 2001]. The nearest CDIP directional wave monitoring sites are: **a) Huntington Beach Array**, Station # 07201; **b) San Clemente**, Station # 05201; **c) Oceanside Array**, Station # 00401. In addition to these CDIP sites waves have been monitored at Torrey Pines Beach from 1972 until 1984 by the SAS Stations deployed by Scripps Institution of Oceanography, (SIO), Pawka (1982). All data sets possessed gaps at various times due to system failure and a variety of start ups

and shut downs and related system maintenance. The undivided data sets were pieced together into a continuous record from 1980-2000 and entered into a structured preliminary data file. The data in the preliminary file represent partially shoaled wave data specific to the local bathymetry around each monitoring site.

To correct these data from the monitoring sites to the nearshore of Encina, they are entered into a refraction/diffraction numerical code, back-refracted out into deep water to remove local refraction and island sheltering effects, and subsequently forward refracted into the immediate neighborhood of Encina. Hence, wave data off each monitoring site was used to hindcast the waves at Agua Hedionda Lagoon.

The backward and forward refractions of CDIP and SIO data to correct it to Encina was done using a numerical refraction-diffraction computer code called OCEANRDS. The primitive equations for this code are lengthy, so a listing of the FORTRAN codes of OCEANRDS appear in Appendix D of the Part 1 study of Jenkins and Wasyl, (2001). These codes calculate the simultaneous refraction and diffraction patterns propagating over a Cartesian depth grid. A large outer grid was used in the back refraction calculations to correct for island sheltering effects, while a high resolution inner grid was used for the forward refraction over the complex bathymetry around Agua Hedionda Lagoon. "OCEANRDS" uses the parabolic equation method (PEM), Radder (1979), applied to the mild-slope equation, Berkhoff (1972). To account for very wide-angle refraction and diffraction relative to the principle wave direction, "OCEANRDS" also incorporates the high order PEM Pade approximate corrections modified from those developed by Kirby (1986a-c). The Pade approximates in "OCEANRDS"

are written in tesseral harmonics, per Jenkins & Inman (1985) in some instances improving resolution of diffraction patterns associated with steep, highly variable bathymetry such as found near the Carlsbad Submarine Canyon. These refinements allow calculation of the evolution and propagation of directional modes from a single incident wave direction; which is a distinct advantage over the more conventional directionally integrated ray methods which are prone to caustics (crossing wave rays) and other singularities in the solution domain where bathymetry varies rapidly over several wavelengths.

Figure 3 gives an example of the forward refraction calculation in the farfield grid, showing wave height variations along an 18.5 km section of coastline including the Oceanside and Carlsbad beach nourishment sites around Agua Hedionda. Figure 3 gives the distribution of wave heights in meters averaged over a 6 hour interval for the extreme event storm the night of 18 January 1988. These were the largest waves of the 20.5 year long simulation period and had 17 sec swells from 270° true with 4.5 meter deep water significant wave heights inside the Catalina Channel off Encina. The wave height contours in Figure 3 are overlaid on the depth contours of the forward refraction grid in units of meters. Refraction diagrams calculated for other extreme events are found in Appendix G of the Part 1 study of Jenkins and Wasyl, (2001). In all of these plots it is noted that the complex shelf bathymetry in the neighborhood of the Carlsbad Submarine Canyon gives rise to refraction patterns with significant variability between "bright spots" (regions of enhanced wave heights) and "shadows" (regions of diminished wave heights). In general, the Carlsbad Submarine Canyon causes a systematic shadow zone at the head of the canyon between Terra Mar and Batiquitos Lagoon, with

progressive bright spots further downcoast of Terra Mar. These alongshore variations in wave height will lead to alongshore variations in longshore transport rates of any constituent, be it sand our brine. These variations are referred to as *divergence of drift*, per Equation (3). A positive divergence of drift (as observed in the Terra Mar region in Figure 3) can lead to offshore transport of surfzone constituents, (Jenkins, et al., 1989, 2002).

The wave height record derived from refraction analysis of the type shown in Figure 3 has been overlaid on the ensemble records of forcing function in Panel-a of Figure 4 for subsequent probability analysis. The average wave height at Encina over this 20.5 year period is 0.87 m while the maximum is 4.51 m occurring during the January 1988 storm, and the minimum is 0.16 m occurring on 17 August 1992 during the building phase of the 1993 El Niño.

B) Currents: While waves dominate the initial dilution and dispersion of heat and concentrated seawater in the inshore domain, the tidal currents control dilution and dispersion in the offshore domain, particularly in the neighborhood of the kelp beds to the south of the power plant. Examples of the three generic categories of tidal circulation on the continental shelf are shown in Figures 3.16 thru 3.18 of the Part 1 study of Jenkins and Wasyl, (2001). A southward net tidal drift is produced by the daily average of all the potential combinations of standing and progressive mixed tides. This net southward drift is an indication that the tidal transport in this region is ***ebb dominated***.

In Panel-b of Figure 4 the daily maximums of the tidal currents on the shelf off Encina are reconstructed over a 20.5 year period form January 1980 through July 2000. The largest daily maximum tidal current during this period was 77.1

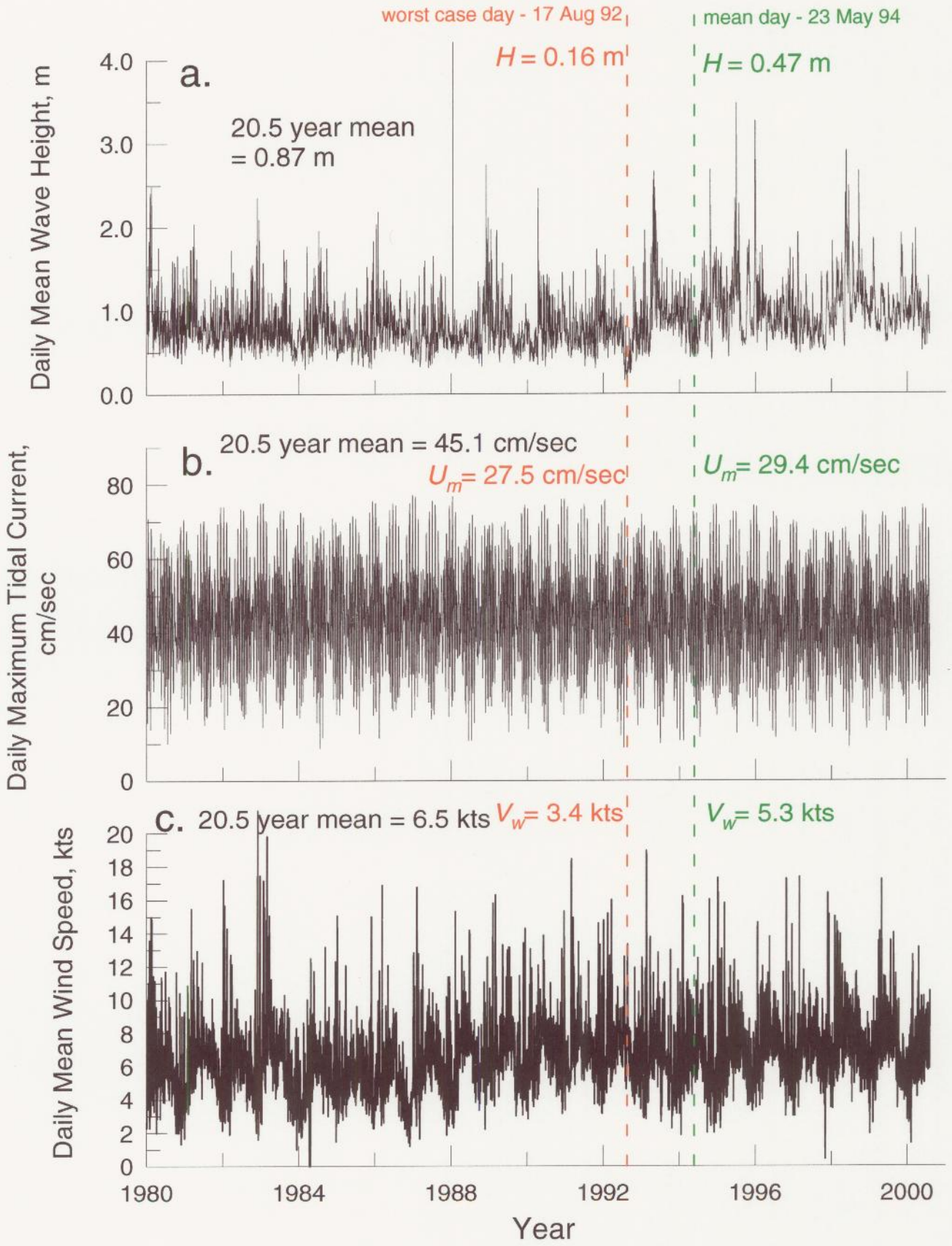

Figure 4. Period of record of forcing functions in the nearfield of Encina Power Plant, 1980-2000.5: a) daily mean wave height, b) daily maximum tidal current velocity, and c) daily mean wind.

cm/sec (1.49 knots) while the smallest daily maximum current was 8.7 cm/sec (0.17 knots). The 20.5 year average daily maximum current in this region is 45.1 cm/sec (0.88 knots).

C) Wind: Daily mean winds from the Scripps Pier Shore Station (SIO,2001) and the Scripps Pier CDIP station (CDIP, 2002) were compiled over the 20.5 year period from January 1980 thru July 2000. This wind record is plotted in Panel-c of Figure 4. Because the lower Southern California Bight is a "wind drought" region due to orographic blocking by the Penninsular Range, the 20.5 year mean wind speed is only 4.9 knots. However, El Niño storms and North Pacific cold fronts episodically increase daily wind speeds with the maximum sustained 24 hour mean wind speed reaching 19.6 knots during the 1997 El Niño storms. The minimum daily mean wind speed is 0 knots. Indeed the coastal winds off Scripps Pier and Encina Power Plant are generally very benign, thereby limiting the degree of wind mixing of the surface water mass.

3.3) Model Scenarios

The 20.5 year long records of the boundary condition variables in Figure 1 and the forcing function variables in Figure 4 were subjected to a joint probability analysis for the simultaneous recurrence of the ***historical extreme case*** combination of these variables and for the average daily combination of these variables (***average case***). The environmental factors for the historical extreme scenarios were prescribed by the search criteria Table 1 below.

Table 1: Search Criteria and Ecological Significance for Historical Extreme Case Combinations of Controlling Environmental Variables.

Variable	Search Criteria	Ecological Significance
Ocean Salinity	Maximize	Higher salinity leads to higher concentrations of RO by-product causing greater stress on marine biology
Ocean Temperature	Maximize	Higher temperature leads to greater stress on marine biology
Ocean Water Levels	Minimize	Lower water levels result in less initial dilution in the discharge channel
Waves	Minimize	Smaller waves result in less mixing in surfzone and less inshore dilution
Currents	Minimize	Weaker currents result in less advection and less offshore dilution
Winds	Minimize	Weaker winds result in less surface mixing and less dilution in both the inshore and offshore

The criteria in Table 1 was applied to a joint probability analysis involving 7,523 historic combinations of ocean salinity, temperature, waves, currents and winds variables, for which the maximization/minimization criteria in Table 1 were enforced.

A) Historical Extreme Case Assignments : The joint probability analysis produced a historical extreme day solution for 17 August 1992. This day is represented by the vertical dashed red line in Figures 5 and 6. The environmental factors of this day were associated with a building El Niño that subsequently climaxed in the winter of 1993. The ocean temperature was 25.0 °C, within 0.1 °C of the 20.5 year maximum. The waves were only 0.16 m, which was the 20.5 year minimum. Winds were 3.4 knots and the maximum tidal current in the offshore domain was only 27.5 cm/sec (0.53 knots). The sluggish tidal current was due to neap tides occurring on this day with a minimum water level of -0.74 ft NGVD. This combination of environmental variables represents a situation that would place maximum thermal stress on the marine biology; and one in which the dilution of the concentrated seawater by-product of the desalination plant would occur very slowly due to minimal ocean mixing. The ocean salinity was 33.51ppt.

Indeed, this was a very hot, calm summer day and the high user demand for electricity had the plant operating close to maximum generating capacity with a flow rate of 725.8 mgd. However, for historical extreme scenarios, this flow rate will be substituted for abnormally low flow rates for these kinds of conditions. We pose 2 hydraulic historical extreme scenarios:

1) ***Unheated Unit 4 Historical Extreme Case*** with two circulation pumps and service water operating for a combined discharge of 304 mgd and $\Delta T = 0$ °C;

2) ***Heated Unit 4 Historical Extreme Case*** with two circulation pumps operating for a combined discharge of 304 mgd and $\Delta T = 5.5$ °C.

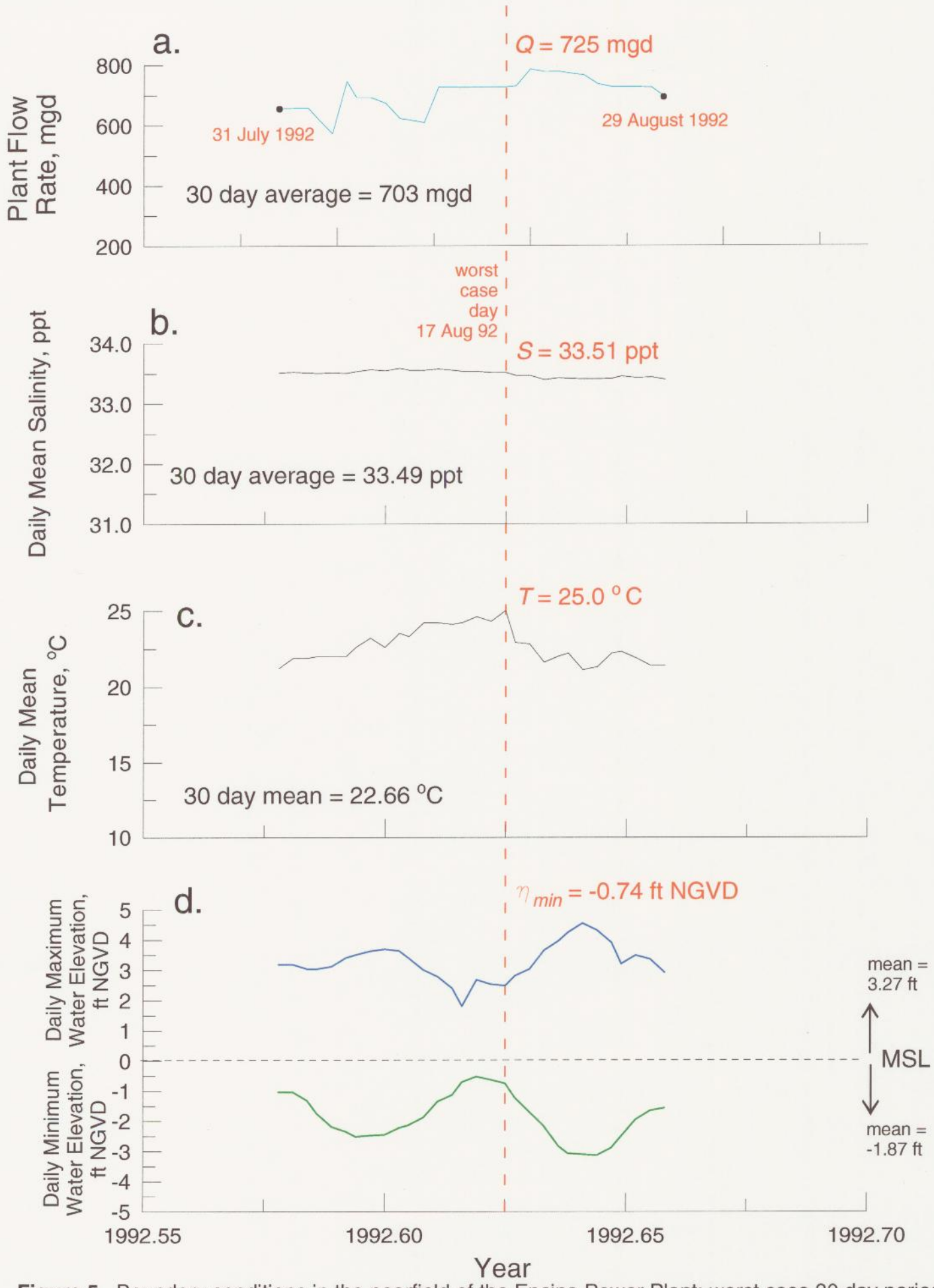

Figure 5. Boundary conditions in the nearfield of the Encina Power Plant: worst case 30 day period: a) plant flow rate, b) daily mean salinity, c) mean temperature, and d) high and low water elevations.

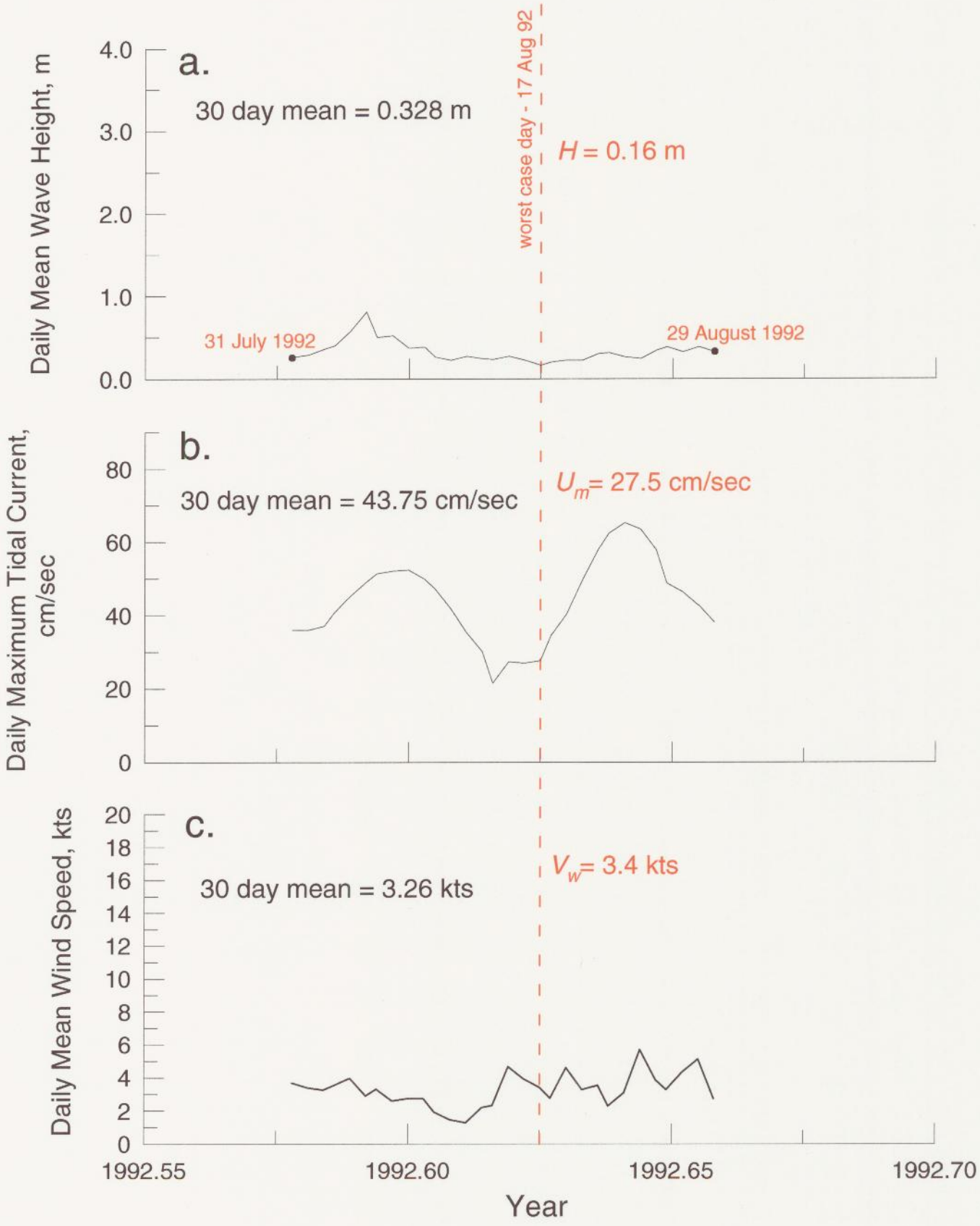

Figure 6. Forcing functions in the nearfield of Encina Power Plant, worst case 30 day period: a) daily mean wave height, b) daily maximum tidal current velocity, and c) daily mean wind.

The abnormally low flow rates of these power plant hydraulic configurations will create the highest possible source strengths of concentrated sea salts and lowest possible initial dilutions "in-the-pipe". They are truly historical extreme cases in a hydraulic sense because they do not allow for the contributions to "in-the-pipe" dilution from the normal salt water service pump flows which typically engage 4 service water pumps, each providing an additional 11 mgd.

B) Average Case Assignments: The average daily combination of the 7 controlling variables over the 20.5 year period of record was found to be represented by the conditions on 23 May 1994. This day is represented in Figures 1 and 4 by the vertical dashed green line. This was a spring day with moderate temperature, winds, waves, and power generation. The Southern Oscillation Index (SOI) was zero indicating that the climate was in a neutral phase. Plant flow rate was 576 mgd, very near the annual mean of 550 mgd (Figure 3.4a). Ocean salinity was 33.52 ppt and ocean temperature was 17.6 °C, both identically the 20.5 year mean. Wave heights were 0.65 m, slightly below the 20.5 year mean, and maximum tidal currents reached 29.4 cm/sec (0.57 knots), also less than the 20.5 year mean. The daily low water level at -1.96 ft NGVD, very close to the mean low tide (MLT). Winds were 5.3 knots, slightly above the 20.5 year mean.

C) Long-Term Simulations from Historic Records: The historic boundary conditions from Figure 1 and the forcing functions from Figure 4 were sequentially input into the model, producing daily solutions for the salinity field discharged from the Encina outfall channel due to the historic operations of the

power plant instead of the historical extreme case hydraulic assumptions. The input stream of seven controlling variables from Figures 4 & 5 produced 7,523 daily solutions for the salinity field around the outfall. A numerical scan of each of these daily solutions searched for the maximum salinity at the outer edge of the ZID, a distance of 1000 ft (305 meters) away from the discharge channel in all directions. The solution scans searched for salinity maximums in both the water column and along the sea floor. For each search, the largest salinity found in any direction away from the outfall was entered into a histogram bin for ultimately assembling a probability density function and cumulative probability from the 7,523 outcomes . These results provided a statistical basis for assessing the likelihood of each of the 4 historical extreme case hydraulic scenarios.

3.4 Calibration

The coupled sets of models were calibrated for end-to-end simulations of known dispersion events off Encina based on temperature depth profile measurements conducted over a nearshore sampling grid during February and March 1989 by Jenkins et al. (1989). This thermal plume data is shown as contour plots in Figure 7 and Appendix A of the Part 1 study of Jenkins and Wasyl, (2001). These thermal plume data were collected as part of an NPDES compliance monitoring program for Encina Power Plant. Initializations for the model were derived from the historic boundary conditions and forcing functions for February and March, 1989 (Figures 1 and 4). Free parameters in the subroutines were adjusted iteratively until a best fit was achieved between the measured and simulated temperature fields.

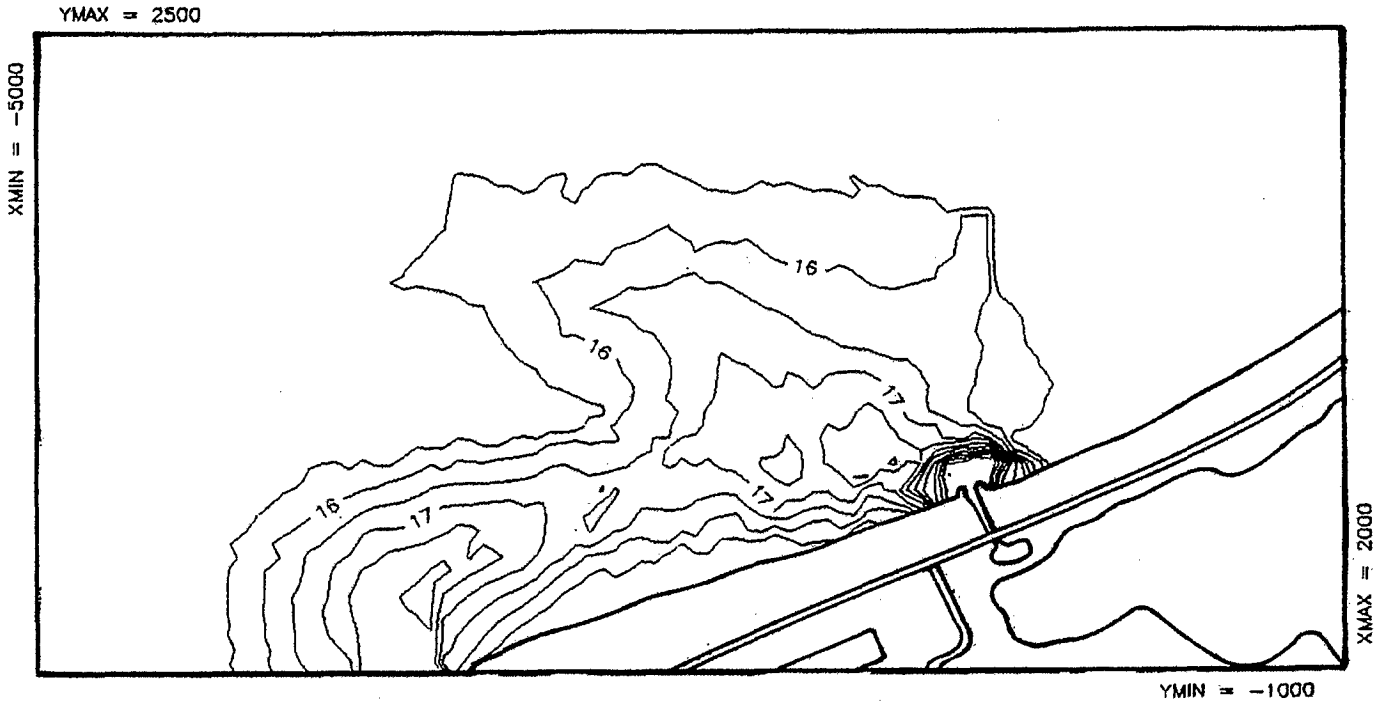

Figure 7. February 28, 1989 temperature distribution two feet below the surface. Temperature is in degrees Centigrade with contours shown at $\frac{1}{2}^0$ C. intervals. Coordinates (x,y) are in feet and relative to an origin at the end of the discharge jetties, see Figure 1.

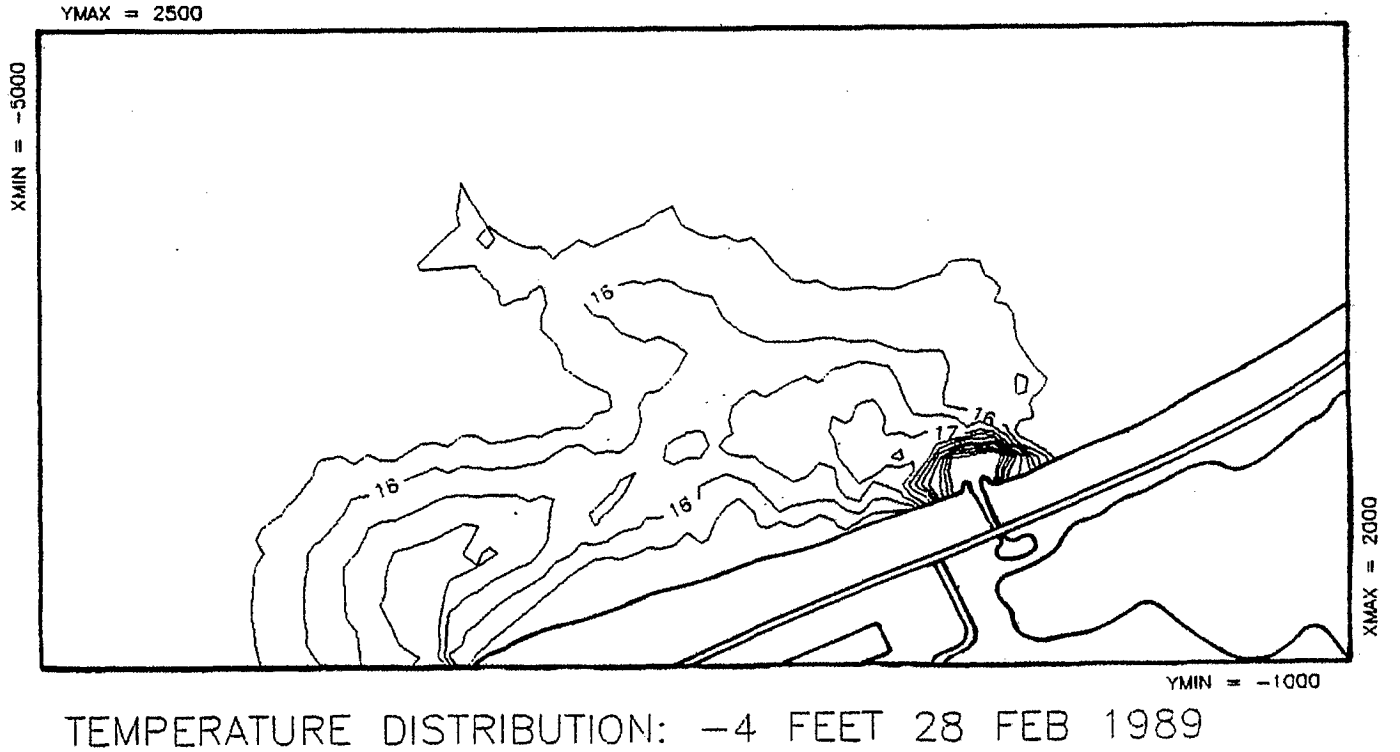

Figure 7. Calibration data [from Jenkins, Skelly, and Wasyl, 1989].

The subroutines of **SEDXPORT-f** contain seven free parameters which are selected by a calibration data set specific to the coastal type for which the hindcast simulation is run. These parameters are as follows according to subroutine:

BOTXPORT·f

*ak2 - stretching factor for vertical eddy diffusivity, ϵ

*ak - adjusts mixing lengths for outfalls

NULLPOINT·f

*ak7 - adjusts the asymmetry of the bedform distribution curve, μ

SURXPORT·f

*aks - adjusts the surf zone suspended load efficiency, K_s

ak4 - stretching factor for the horizontal eddy diffusivity, ϵ_x

RIVXPORT·f

*ak3_1 - adjusts the jetty mixing length and outfall mixing lengths

*ak3 - stretching factor for the horizontal eddy diffusivity of the river plume, ϵ_H

The set of calibration values for these parameters was used without variation or modification for all model scenarios. Figure 3.23 of the Part 1 study of Jenkins and Wasyl, (2001) shows the measured surrogates for historical extreme case and average case scenarios measured during the 1989 field monitoring efforts. Figure 2.23 Panel-a of the Part 1 study of Jenkins and Wasyl, (2001) is the historic extreme observed case measured on 7 March 1989 with the power plant operating at its maximum flow rate of 808 mgd with a maximum certified Delta-T of 20 °F (11 °C). This set of measurements provided an upper limit of the maximum heat

output and size of the thermal footprint under existing conditions. The area inside the 2 °F (1.1 °C) temperature anomaly contour was measured at 113 acres. Panel-b of Figure 3.23 of the Part 1 study of Jenkins and Wasyl, (2001) gives the representative average case scenario measured on 28 February 1989 with the plant operating at 738.9 mgd and a Delta-T of 10 °F (5.5 °C). The footprint of the 2 °F (1.1 °C) temperature anomaly contour was measured at 65 acres. It was found that the thermal plume deflects downcoast to the south in the direction of net transport for both historical extreme cases and average case and for all other cases in Appendix A of the Part 1 study of Jenkins and Wasyl, (2001).

4) Results

For each historical extreme scenario, results are presented in terms of four principle model outputs: 1) salinity of the combined discharge on the sea floor, 2) depth averaged salinity of the combined discharge , 3) dilution factors for the raw concentrate at the sea floor, and 4) depth averaged dilution factors for the raw concentrate in the water column. For the "heated " scenarios ($D = 5.5^0$ C) additional out puts are given for: 5) the temperature of the combined discharge on the sea floor, and 6) the depth averaged temperature of the combined discharge in the water column.

Salinity fields are contoured in parts per thousand (ppt) according to the color bar scale at the bottom of each plot. For purposes of comparing scenarios, the salinity scale range spans from 33.5 ppt to 55.0 ppt. Ambient ocean salinity is stated in the caption of each salinity field plot. Of particular interest in the outcome of each historical extreme scenario will be areas in which the discharge plume elevates the local salinity above 37 ppt.

The dilution fields are contoured in base-10 log according to the color bar scale at the bottom of each plot, with a scale range that spans from 10^0 to 10^7. We are particularly concerned about the dilution factor of the raw concentrate in the water column at the edge of the ZID, 1000 ft in any direction from the mouth of the discharge channel. The present NPDES permit for the thermal effluent requires a dilution factor of 15 to 1 at the edge of the ZID, and this standard may likely be applied to the hyper-saline discharge of the desalination plant.

Temperature fields are contoured in degrees Celsius according to the color bar scale at the bottom of each plot. The temperature scale range spans from 17.5^0 C to 28.5^0 C. Ambient ocean temperature is stated in the caption of each temperature field plot. For the temperature field of the heated historical extreme cases, it is important that none of the water quality objectives as stated in Section 3.1E are violated.

4.1) Unheated Unit 4 Historical Extreme Case

Two Unit 4 circulation pumps are assumed to be operating at a combined 304 mgd, with two supplemental service water pumps. After blending with the concentrated sea salts discharged from the desalination plant the combined discharge exiting the discharge channel is 254 mgd. No power generation is also assumed so that the Delta-T is $\Delta T = 0^0$ C. End-of-pipe salinity is 40.11 ppt, diluted by a factor of 5.1 to 1 from an initial salinity of 67.02 ppt for the raw concentrate.

Figure 8 gives the salinity field on the sea floor resulting from the Unit 4 historical extreme hydraulic case for unheated discharge. The salinity field is averaged over a 24 hour period .The inner core of the hyper-saline bottom boundary layer is at 39 ppt but covers an area of 2.4 acres of the sub-tidal beach face. Offshore, the density flow of the bottom boundary layer due to elevated salinity follows a southward trajectory and covers about 44 acres of benthic environment with elevated salinity 10 % above ambient ocean conditions. Maximum bottom salinity at the edge of the ZID is 38.2 ppt, found 1000 ft offshore to the southwest of the discharge channel. Depth averaged salinities in

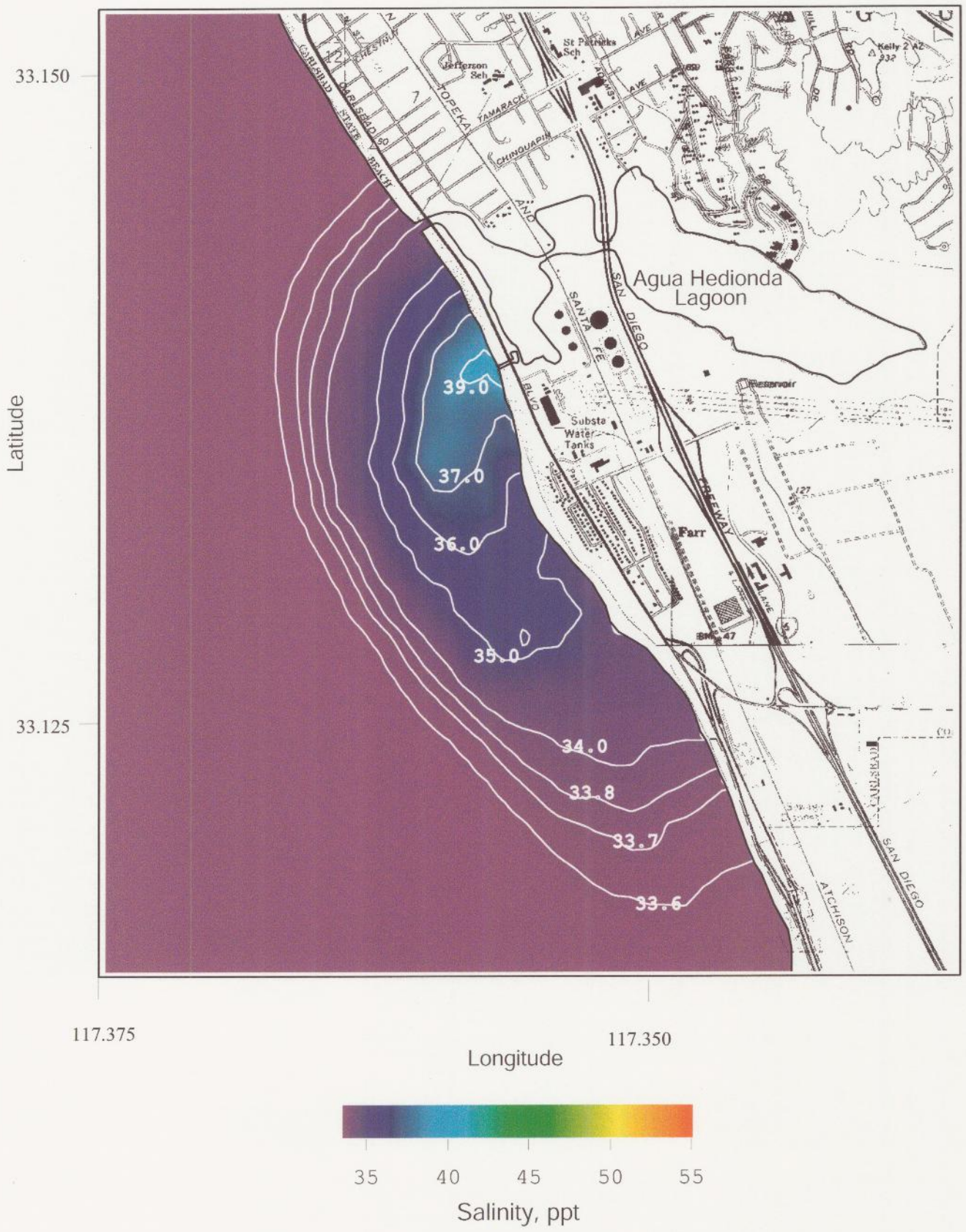

Figure 8. Historical extreme conditions for Unit 4 with 2 pumps, unheated ($\Delta T = 0\ ^{o}C$). Daily average of the bottom salinity of concentrated seawater for R.O. = 50 mgd, plant inflow rate = 304 mgd, combined discharge = 254 mgd, ambient ocean salinity = 33.51 ppt, ocean conditions, 17 Aug 1992.

Figure 9 are found to be everywhere less than 10% over ambient. Depth averaged water column salinities are at most 36.0 ppt. Maximum water column salinity at the edge of the ZID is 35.2 ppt.

Bottom dilution factors for the raw concentrate are shown in Figure 10 for the "unheated" Unit 4 historical extreme case. Minimum dilution on the sea bed at the edge of the ZID is 7.1 to 1 and dilutions are less than 15 to 1 on 42 acres of surf zone bottom and offshore seabed. However, Figure 11 shows that in the water column, where 316(A) minimum dilution permit standards apply, dilutions improve to 19.8 to 1 at the edge of the ZID, comfortably above the 15 to 1 minimum standard. Therefore, from both a salinity tolerance and regulatory perspective, the unheated Unit 4 historical extreme case is acceptable.

4.2) Heated Unit 4 Historical Extreme Case

Two Unit 4 circulation pumps are assumed to be operating at 304 mgd combined flow rate, with no auxiliary service water and a Delta-T of $\Delta T = 5.5^0$ C. End-of-pipe salinity is 40.11 ppt, diluted by a factor of 5.1 to 1 from an initial salinity of 67.02 ppt for the raw concentrate.

Figure 12 gives the salinity field on the sea floor resulting from the Unit 4 historical extreme case for heated discharge. The increased thermal agitation introduced into the combined discharge by the thermal effluent increases the mixing and assimilation of the concentrated sea salts by the receiving water. The thermal effluent also renders the combined effluent less negatively buoyant, reducing the percent increase in density to 0.4%. Consequently, the inner core of the hyper-saline bottom boundary layer is greatly diminished and nowhere outside

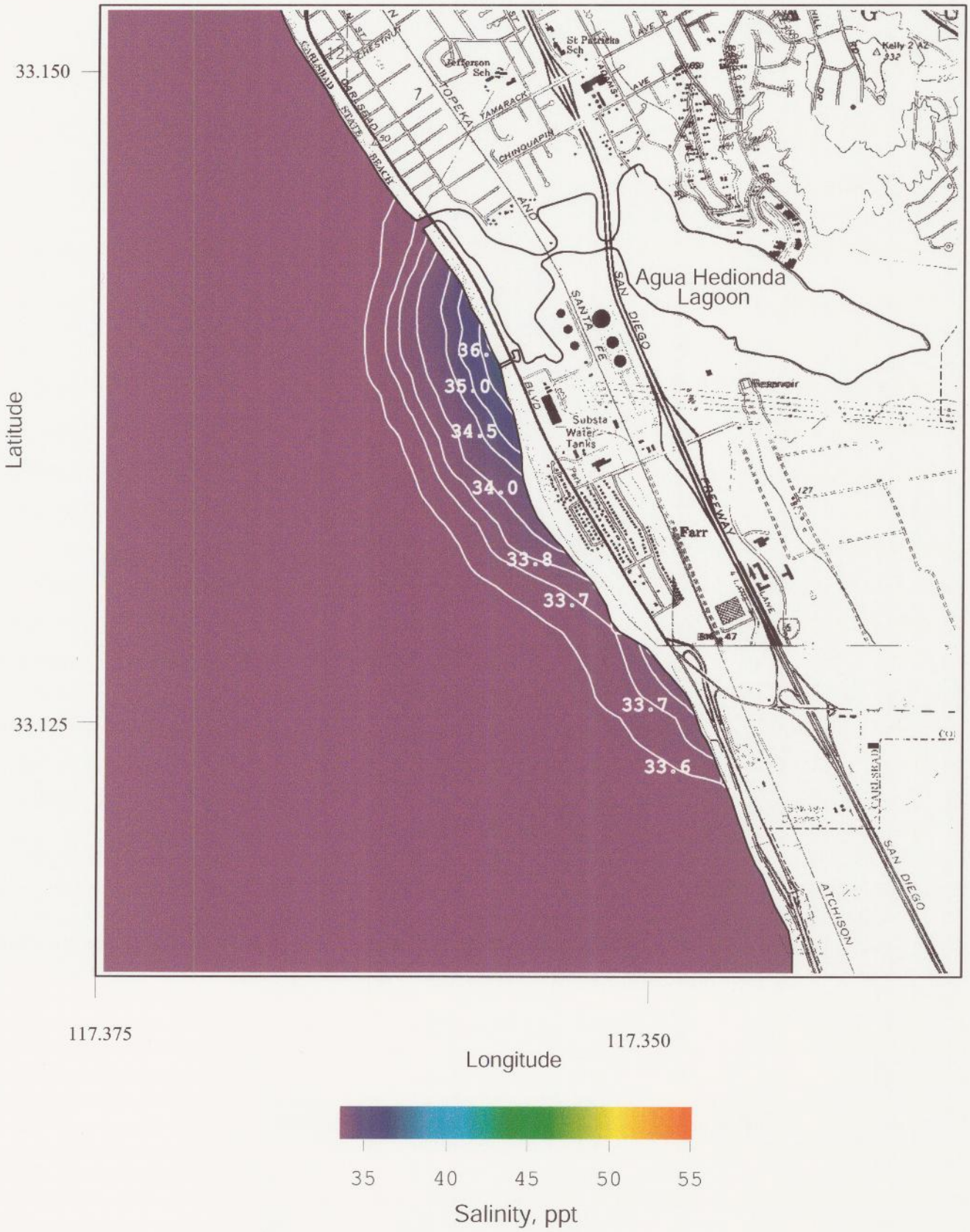

Figure 9. Historical extreme conditions for Unit 4 with 2 pumps, unheated ($\Delta T = 0$). Daily depth-averaged salinity of concentrated seawater for R.O. = 50 mgd, plant inflow rate = 304 mgd, combined discharge = 254 mgd, ambient ocean salinity = 33.51 ppt, ocean conditions, 17 Aug 1992.

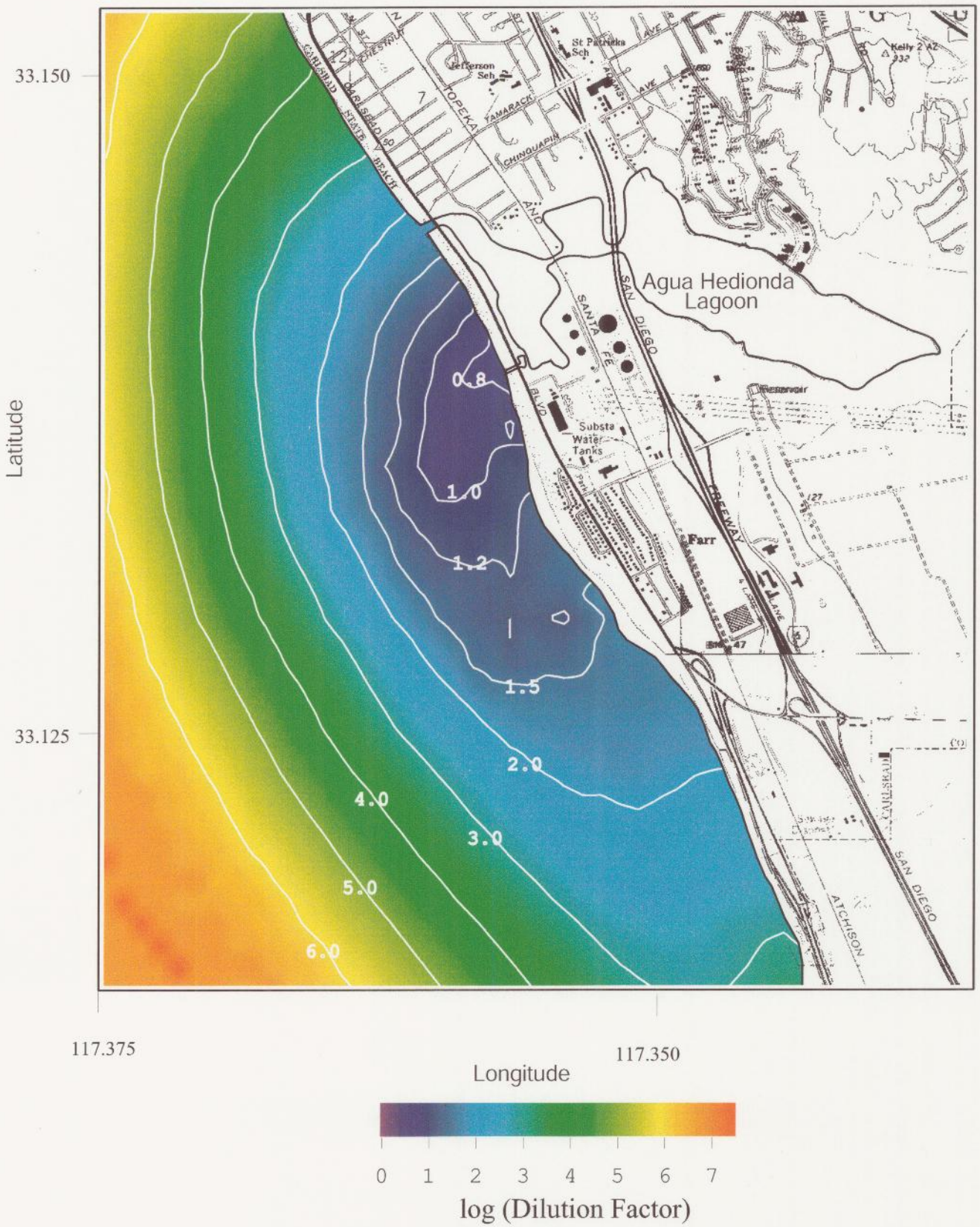

Figure 10. Historical extreme conditions for Unit 4 with 2 pumps, unheated ($\Delta T = 0$). Seafloor dilution factor for raw concentrate from desalination. R.O. = 50 mgd, plant inflow rate = 304 mgd, combined discharge = 254 mgd, ambient ocean salinity = 33.51 ppt, ocean conditions, 17 Aug 1992.

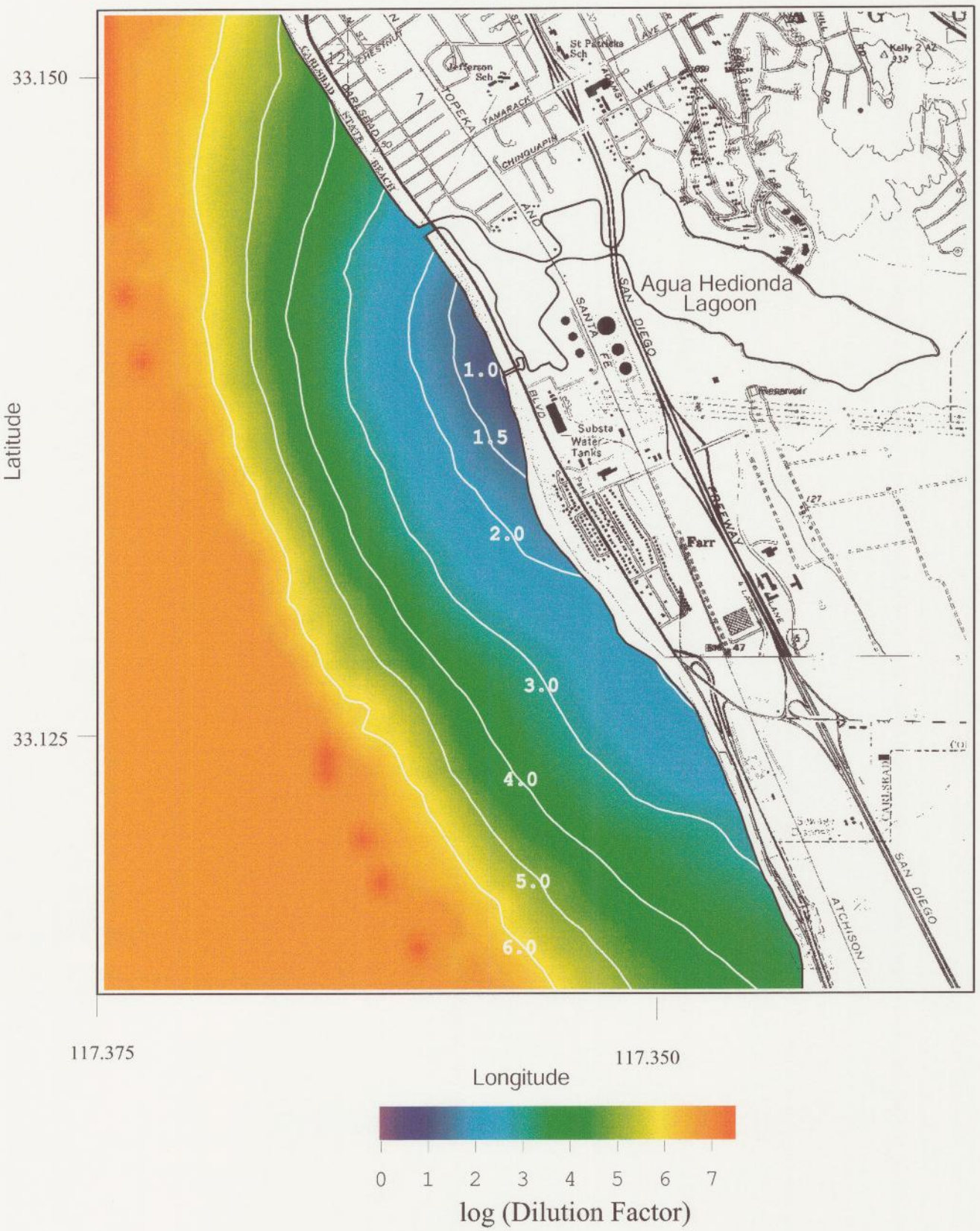

Figure 11. Historical extreme conditions for Unit 4 with 2 pumps, unheated ($\Delta T = 0$). Depth-averaged dilution factor for raw concentrate from desalination. R.O. = 50 mgd, plant inflow rate = 304 mgd, combined discharge = 254 mgd, ambient ocean salinity = 33.51 ppt, ocean conditions, 17 Aug 1992.

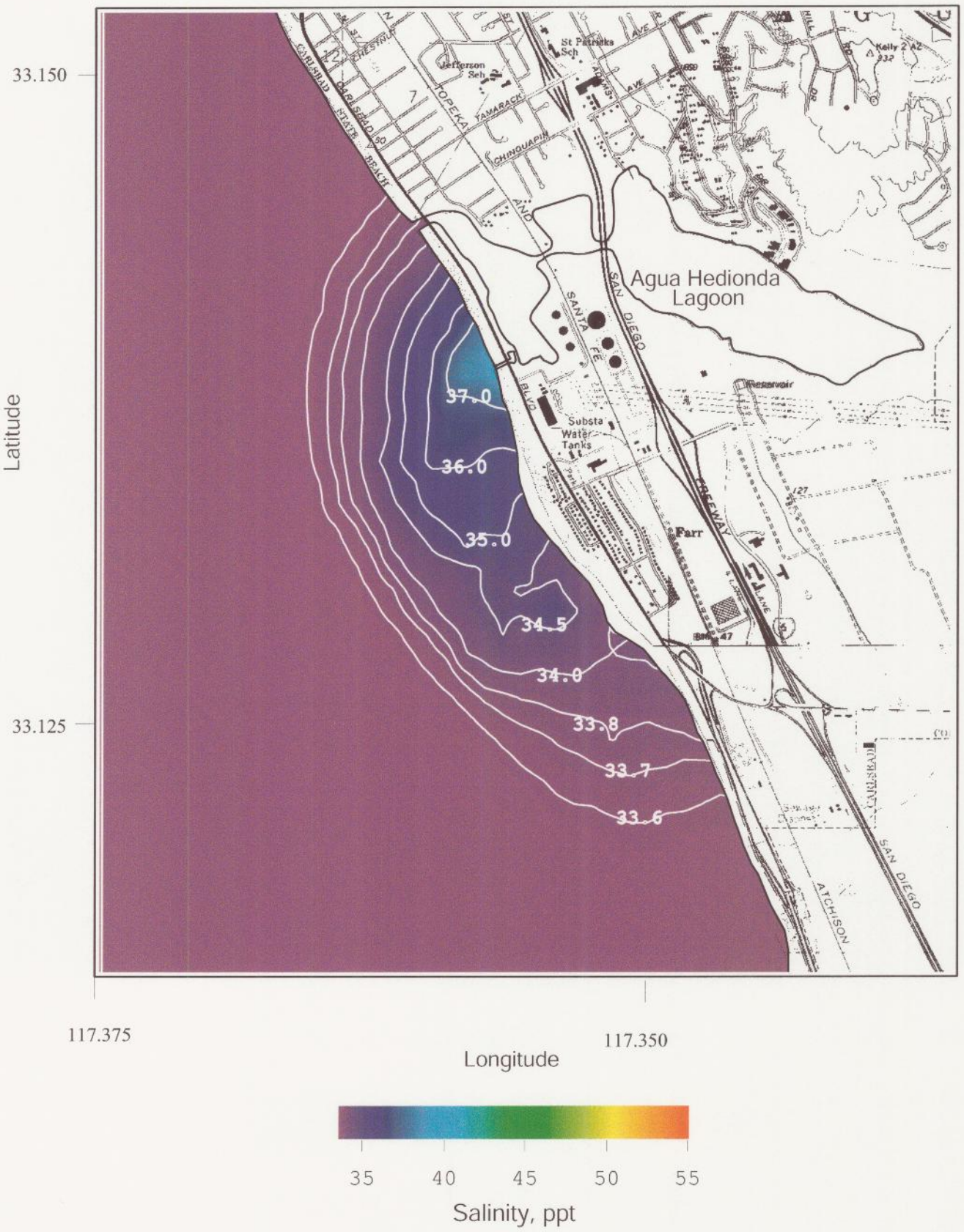

Figure 12. Historical extreme conditions for Unit 4 with 2 pumps, heated ($\Delta T = 5.5\ ^{o}C$). Daily average of the bottom salinity of concentrated seawater for R.O. = 50 mgd, plant inflow rate = 304 mgd, combined discharge = 254 mgd, ambient ocean salinity = 33.51 ppt, ocean conditions, 17 Aug 1992.

the discharge channel does the salinity exceed 40 ppt. The salinity maximum of 37.9 ppt covers an area of less than on acre of the sub-tidal beach face. Maximum bottom salinity at the edge of the ZID is 36.3 ppt, 1000 ft offshore to the southwest of the discharge channel. About 15 acres of seabed are subjected to salinities exceeding ambient levels by 10 % or more. No where does the depth averaged salinity exceed ambient levels by more than 10 % (see Figure 13). Depth averaged water column salinities are at most 36.1 ppt over a region of 1.6 acres of surf zone. Maximum water column salinity at the edge of the ZID is 34.9 ppt in the surf zone south of the discharge channel.

Bottom dilution factors for the raw concentrate are shown in Figure 14 for the "heated" Unit 4 historical extreme case. Minimum dilution on the sea bed at the edge of the ZID is 12.0 to 1. Dilutions are less than 15 to 1 on 12 acres of surf zone bottom and offshore seabed, a significant improvement over all other historical extreme scenarios. In the water column (Figure 15), dilutions are a robust 24.1 to 1 at the edge of the ZID, significantly better than the 15 to 1 required for the thermal effluent under existing 316(A) permits. From both a salinity tolerance and regulatory perspective, the heated Unit 4 historical extreme case passes with a considerable safety margin, even with minimal contribution of service water in the hypothetical formulation of the scenario.

The bottom temperature field for the heated Unit 4 hydraulic historical extreme case is plotted in Figure 16. This figure shows that for a warm El Nino summertime ocean, the water quality objectives stated in Section 3.1E are satisfied. The 27^0 C isotherm (delineating the 2^0 C temperature anomaly) makes contact with the bottom only at the mouth of the discharge channel and never

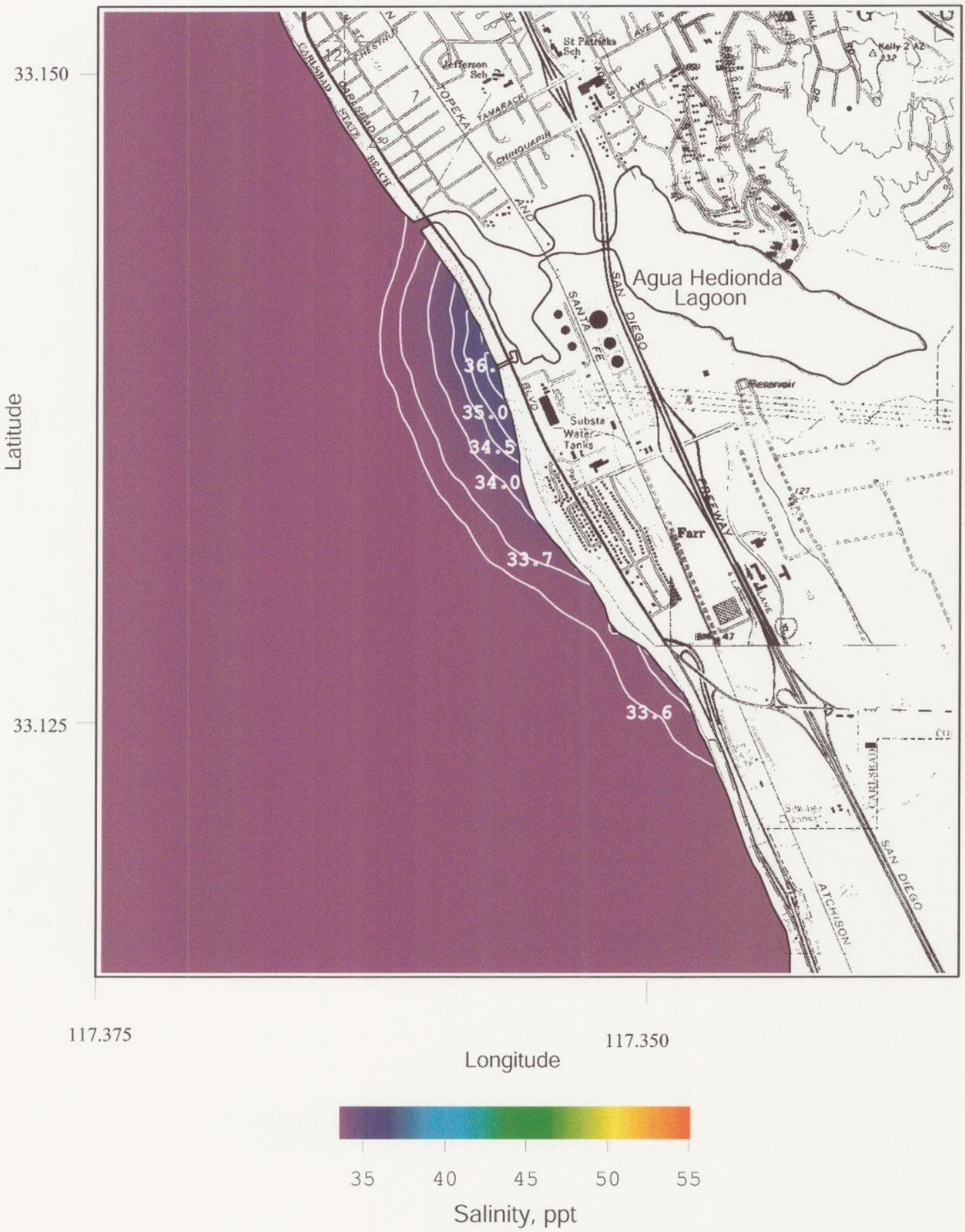

Figure 13. Historical extreme conditions for Unit 4 with 2 pumps, heated ($\Delta T = 5.5\ ^{o}C$). Daily depth-averaged bottom salinity of concentrated seawater for R.O. = 50 mgd, plant inflow rate = 304 mgd, combined discharge = 254 mgd, ambient ocean salinity = 33.51 ppt, ocean conditions, 17 Aug 1992.

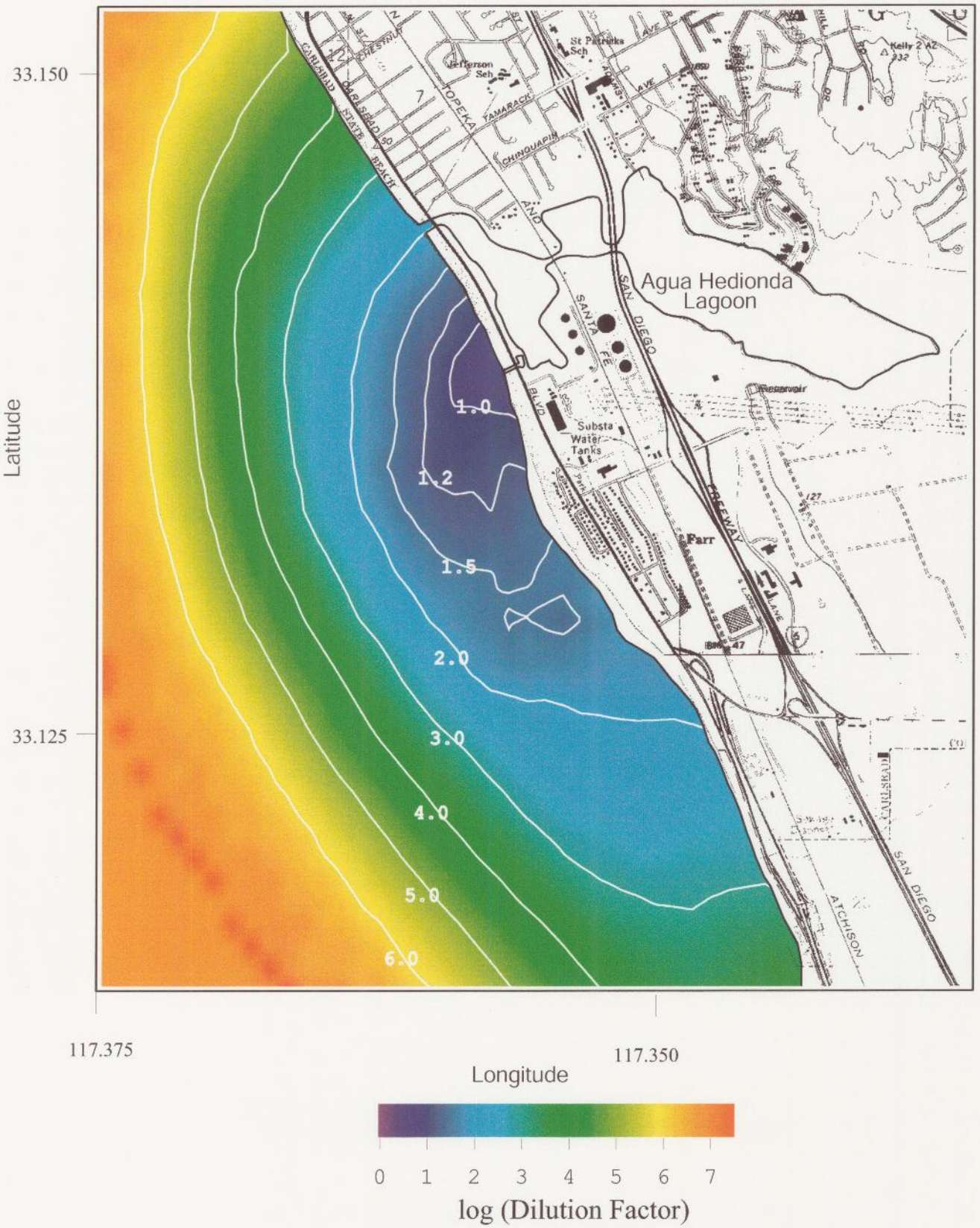

Figure 14. Historical extreme conditions for Unit 4 with 2 pumps, heated ($\Delta T = 5.5\ ^{o}C$). Seafloor dilution factor for raw concentrate from desalination. R.O. = 50 mgd, plant inflow rate = 304 mgd, combined discharge = 254 mgd, ambient ocean salinity = 33.51 ppt, ocean conditions, 17 Aug 1992.

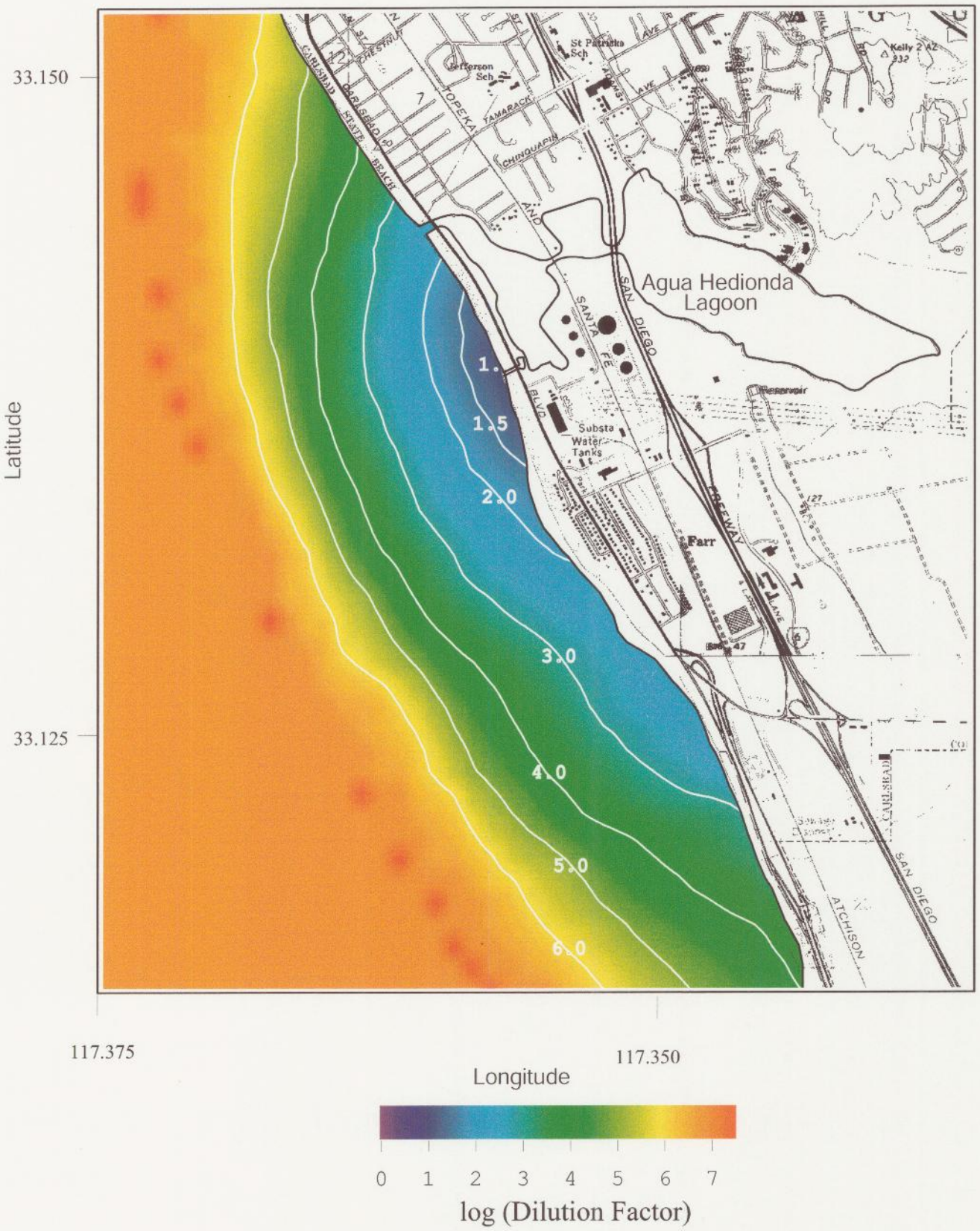

Figure 15. Historical extreme conditions for Unit 4 with 2 pumps, heated ($\Delta T = 5.5\ ^{o}C$). Depth-averaged dilution factor for raw concentrate from desalination. R.O. = 50 mgd, plant inflow rate = 304 mgd, combined discharge = 254 mgd, ambient ocean salinity = 33.51 ppt, ocean conditions, 17 Aug 1992.

Figure 16. Historical extreme conditions for Unit 4 with 2 pumps, heated ($\Delta T = 5.5\ ^{o}C$). Daily average of the bottom temperature of concentrated seawater for R.O. = 50 mgd, plant inflow rate = 304 mgd, combined discharge=254 mgd, ambient ocean temperature = 25.0 ^{o}C, ocean conditions, 17 Aug 1992.

comes close to the edge of the ZID. The depth averaged temperatures in Figure 17 are everywhere less than 1.0^0 C over ambient, and therefore satisfy the requirements of the existing 316(A) permit requirements.

4.3) Historical Average Hydraulic Case

The model simulation of the 24 hour average of the salinity field on the seabed is plotted in Figure 18 during the average day conditions for an RO production rate of 50 mgd and a plant flow rate of 576 mgd. Because the combined discharge (at 526 mgd) is heavier than seawater, Figure 19 delineates the maximum saline impacts found anywhere in the water column on an average day. Maximum bottom salinities reach 36.0 ppt directly offshore of the discharge. Therefore, no benthic area is exposed to salinities in excess of 36 ppt. Maximum bottom salinities at the edge of the ZID reach only 34.4 ppt, the natural upper limit of seasonal variability in the local salinity field. The depth-averaged salinity field is plotted in Figure 19 for RO production at 50 mgd during the average day conditions. Maximum depth-averaged salinities reach 34.4 ppt directly seaward of the mouth of the discharge channel. Therefore, no water column saline impacts exceed 10% and the maximum water column salinity at the edge of the ZID reaches only 34.0 ppt.

The corresponding dilution fields of the raw concentrate on the seabed are plotted in Figure 20, while those fields depth averaged in the water column are found in Figure 21. The minimum dilution of bottom salinity at the edge of the ZID (distance of 1000 ft (305 m) in any direction from the discharge channel) is

Figure 17. Historical extreme conditions for Unit 4 with 2 pumps, heated ($\Delta T = 5.5\ ^{o}C$). Daily depth-averaged temperature of concentrated seawater for R.O. = 50 mgd, plant inflow rate = 304 mgd, combined discharge=254 mgd, ambient ocean temperature = 25.0 ^{o}C, ocean conditions, 17 Aug 1992.

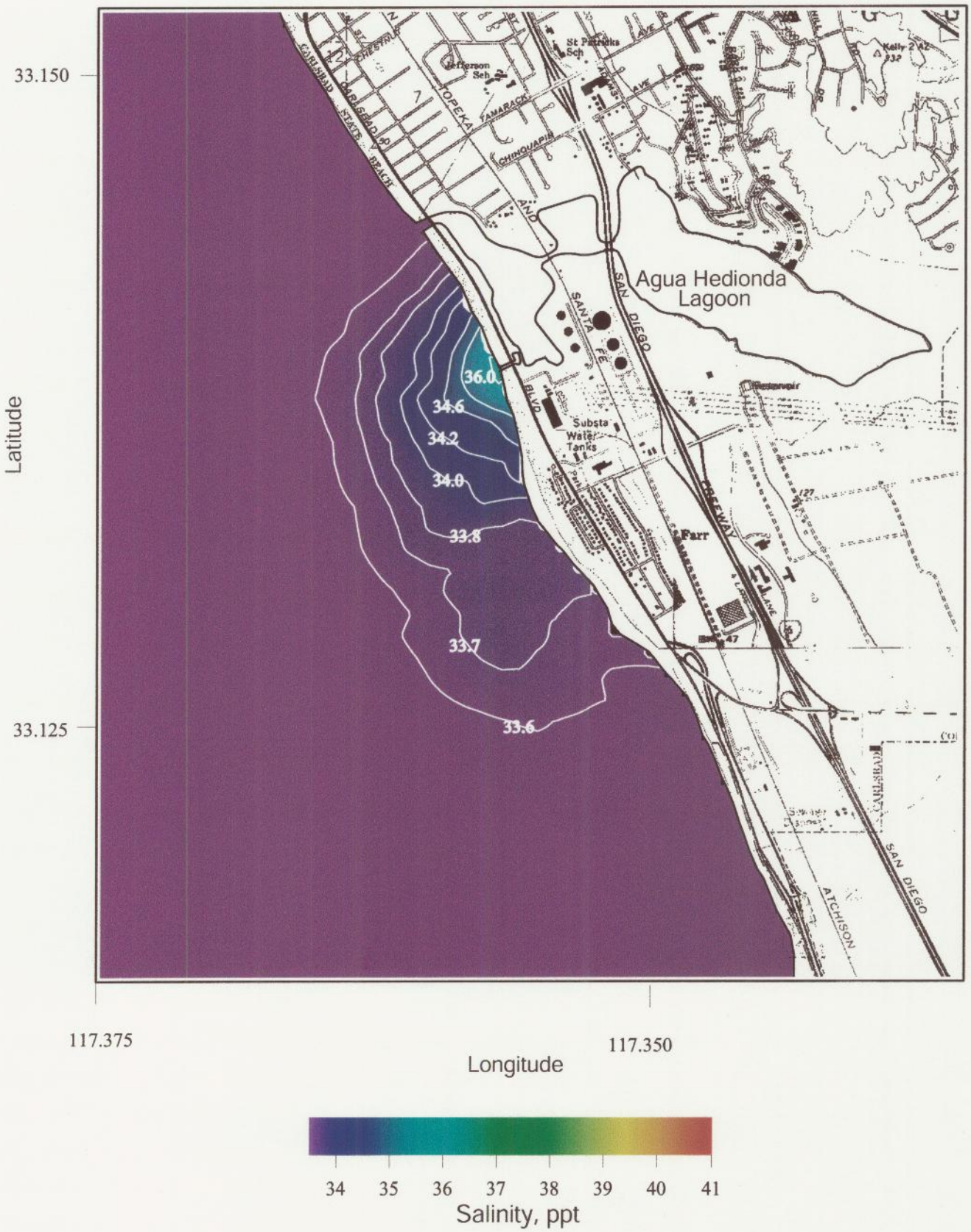

Figure 18. Historical average hydraulic case, heated ($\Delta T = 5.5^{o}$ C). Daily average of the bottom salinity of concentrated seawater for R.O. = 50 mgd, plant inflow rate = 576 mgd, combined discharge = 526 mgd, ambient ocean salinity = 33.52 ppt, ocean conditions, 23 May 1994.

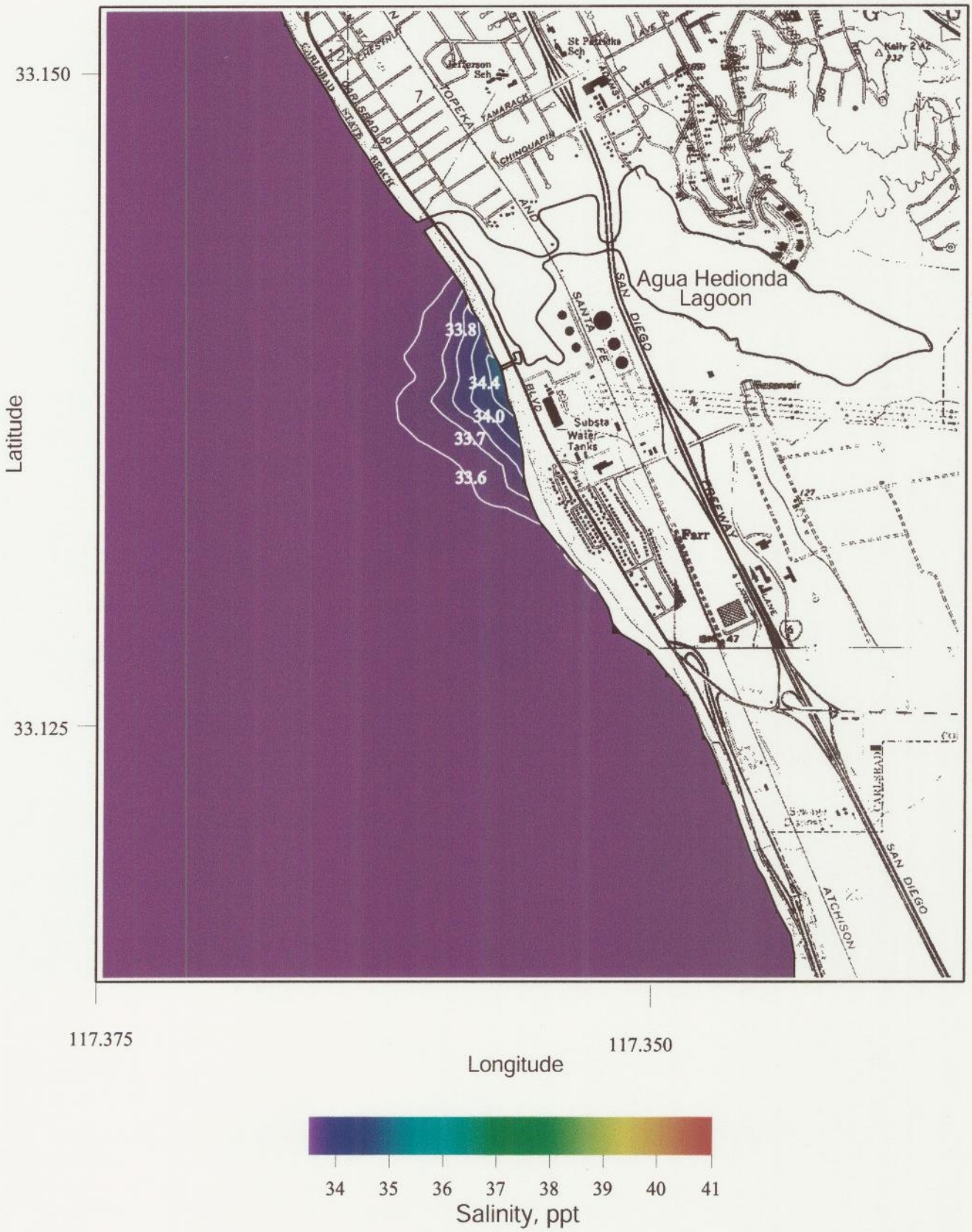

Figure 19. Historical average hydraulic case ($\Delta T = 5.5^{o}$ C). Daily depth-averaged salinity of concentrated seawater for R.O. = 50 mgd, plant inflow rate = 576 mgd, combined discharge = 526 mgd, ambient ocean salinity = 33.52 ppt, ocean conditions, 23 May 1994.

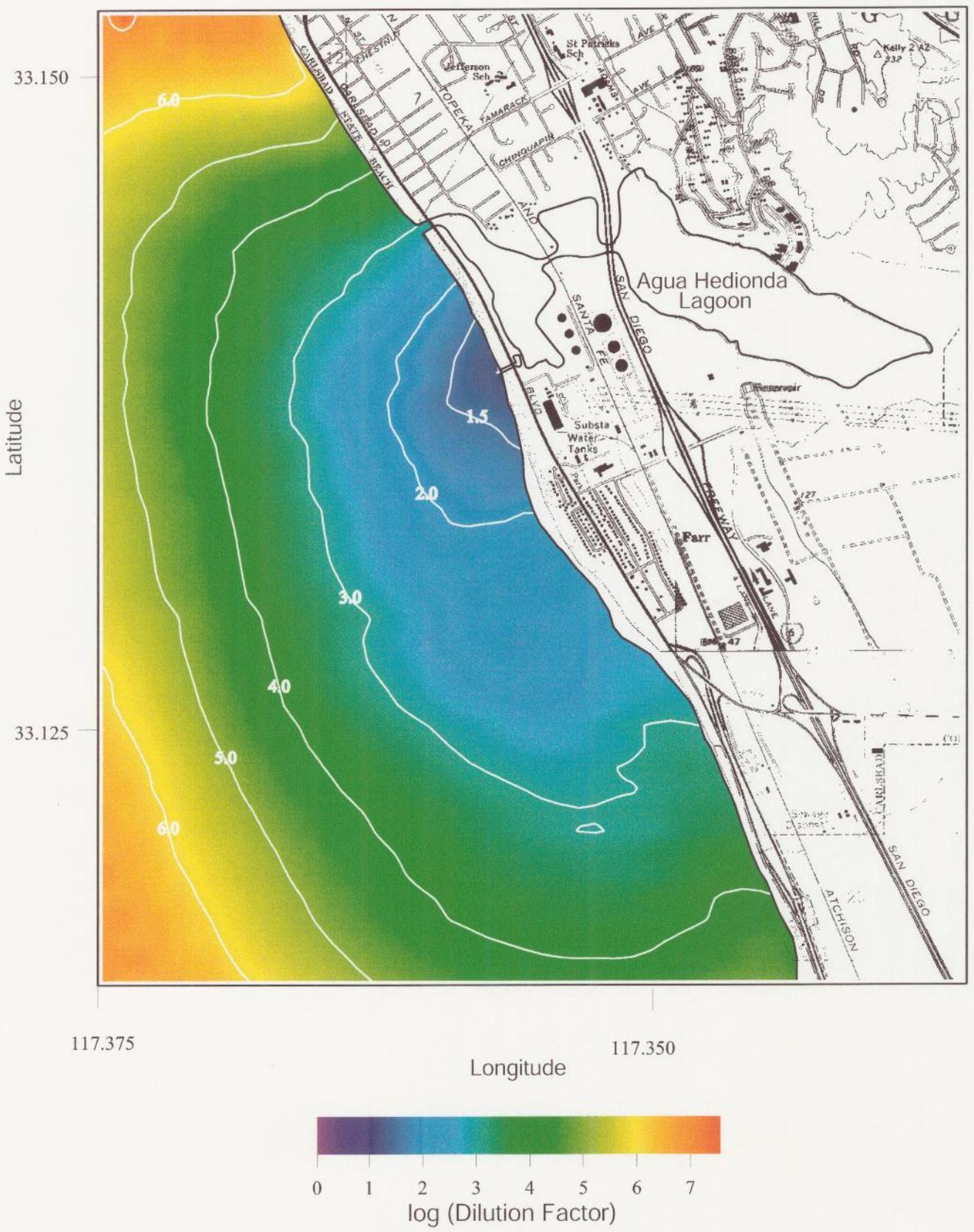

Figure 20. Historical average hydraulic case ($\Delta T = 5.5^{o}$ C). Seafloor dilution factor for raw concentrate from desalination. R.O. = 50 mgd, plant inflow rate = 576 mgd, combined discharge = 526 mgd, ambient ocean salinity = 33.52 ppt, ocean conditions, 23 May 1994.

32 to1. In the water column, the minimum dilution at the edge of the ZID is 68.4 to 1.

The model simulation of the average case temperature field on the seabed is plotted in Figure 22. The "end of the pipe" discharge temperature is 23.1 °C with a salinity of 36.71 ppt. Over a 24 hour period the maximum temperature in the discharge channel is 21.0 °C. No area of seabed beyond the discharge channel experiences a 4 °F (2.2 °C) increase in bottom temperature. Maximum seabed temperature is 19.3 immediately offshore of the discharge jetties. The maximum temperature 1000 ft (305 m) from the discharge channel in any direction is only 1.45 °F (0.8 °C) above ambient ocean temperatures. The depth-averaged temperature field is plotted in Figure 23 for average case conditions. Because the combined discharge is heavier than ambient seawater, elevated temperatures within the water column are less and the thermal footprint is much smaller than what was found on the seabed in Figure 22. Maximum depth-averaged temperatures reach 18.9 °C directly seaward of the mouth of the discharge channel. It is apparent that the concentrated seawater under average day conditions has caused the maximum thermal footprint to move to the seafloor. The seabed footprint of the 2 °F temperature anomaly (18.7 °C contour) is 9 acres. This compares with 65 acres for the existing 2 °F maximum footprint found on the sea surface under average case conditions during the 1989 field measurements (see Section 3.5 and Appendix A of Jenkins and Wasyl, 2001). Therefore, acceptable salinity regimes are achieved under average conditions and water quality objectives set for thermal effluent are also satisfied.

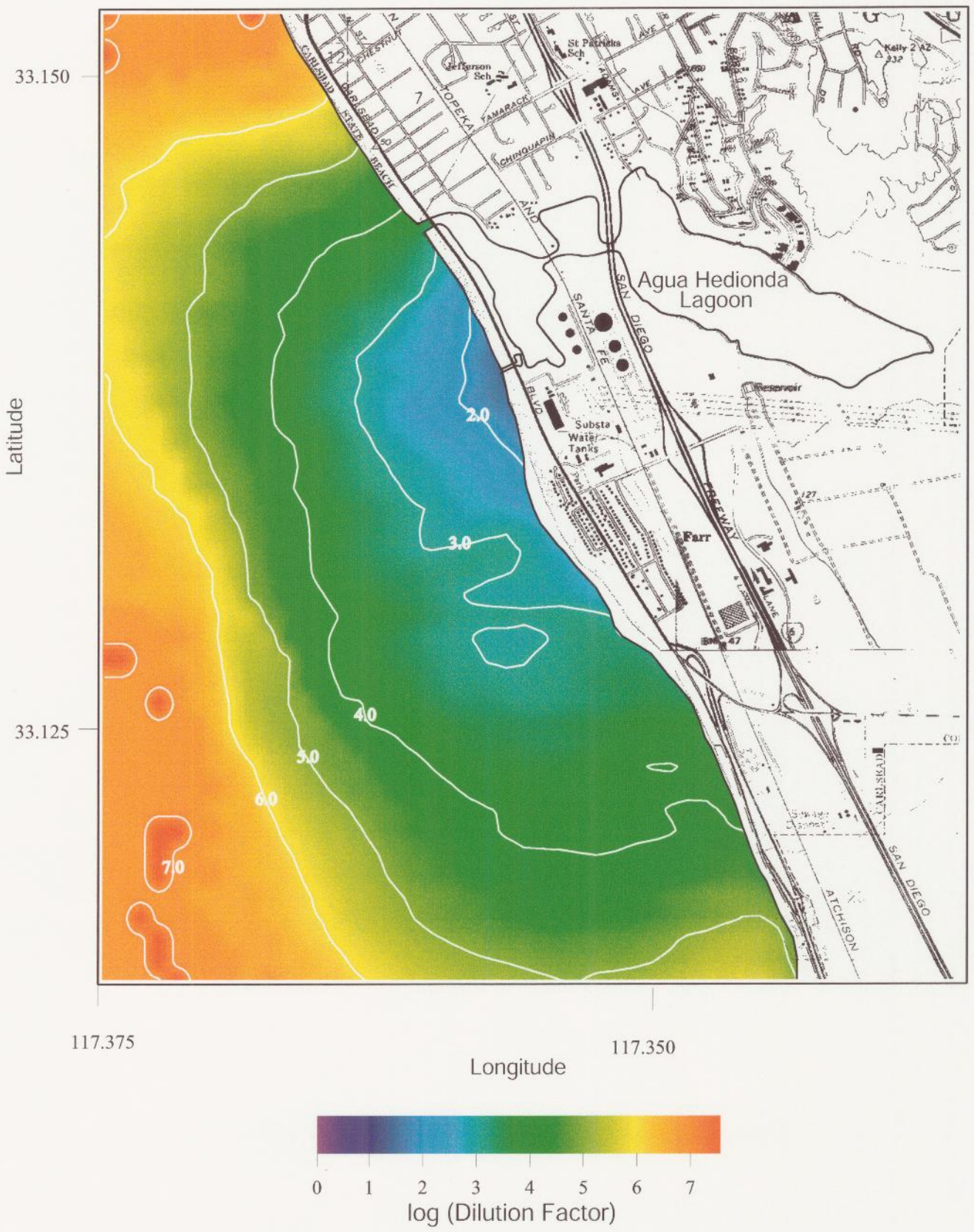

Figure 21. Historical average hydraulic case ($\Delta T = 5.5^{o}$ C). Depth-averaged dilution factor for raw concentrate from desalination. R.O. = 50 mgd, plant inflow rate = 576 mgd, combined discharge = 526 mgd, ambient ocean salinity = 33.52 ppt, ocean conditions, 23 May 1994.

Figure 22. Historical average hydraulic case ($\Delta T = 5.5^{o}$ C). Daily average of the bottom temperature of concentrated seawater for R.O. = 50 mgd, plant inflow rate = 576 mgd, combined discharge = 526 mgd, ambient ocean temperature = 17.6 °C, ocean conditions, 23 May 1994.

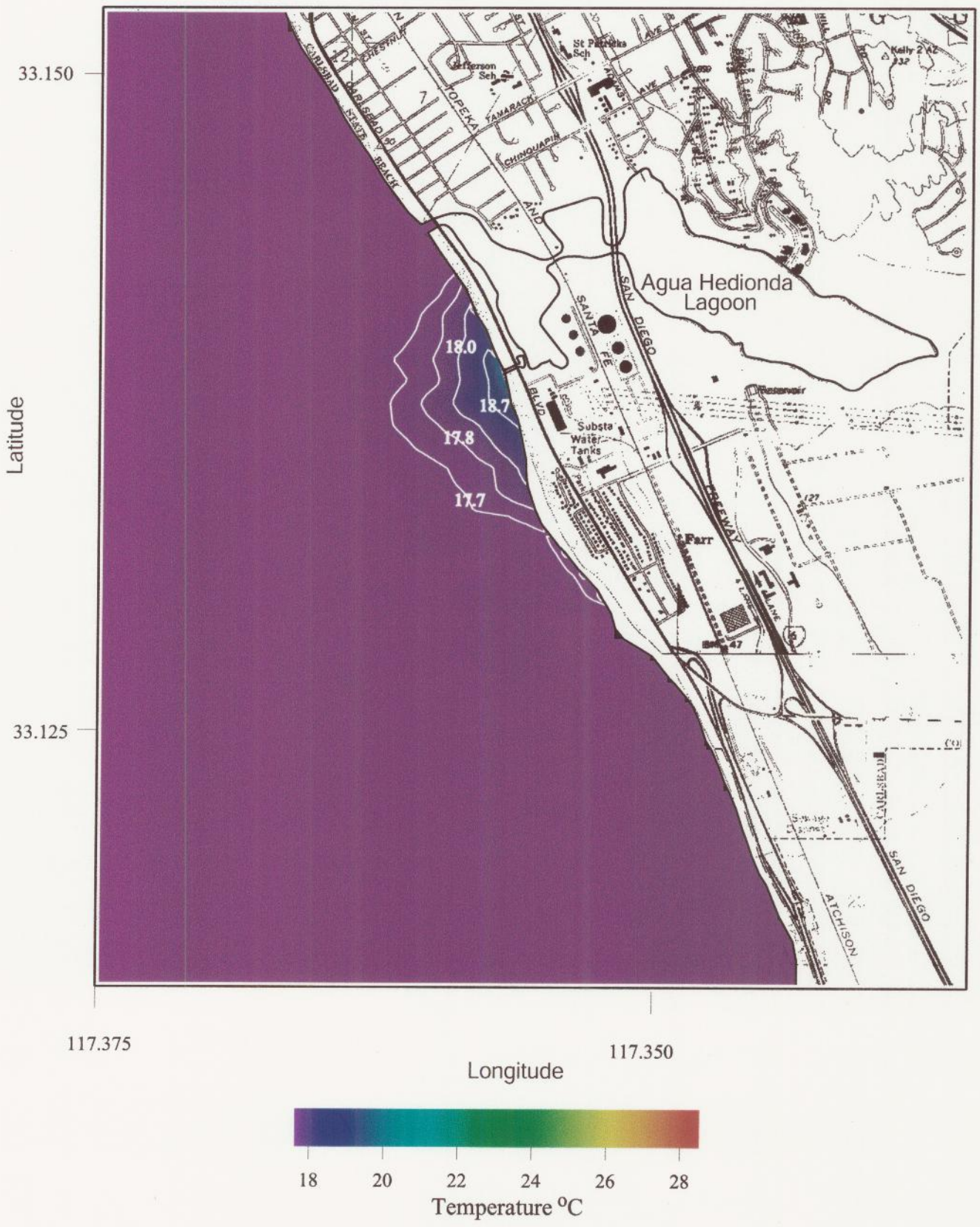

Figure 23. Historical average hydraulic case ($\Delta T = 5.5^{o}$ C). Daily depth-averaged temperature of concentrated seawater for R.O. = 50 mgd, plant inflow rate = 576 mgd, combined discharge = 526 mgd, ambient ocean temperature = 17.6 °C, ocean conditions, 23 May 1994.

4.4) Historical Extremes Versus Long-Term Outcomes

When the local salinity variation and historic plant flow rates in Figure 1 are applied to the desalination process a considerable range in end-of-pipe salinities results over the long term (eg. 20-yr periods). Figure 24 shows a sensitivity analysis of how end-of pipe salinities will decline with increasing power plant flow rates when the desalination plant is producing product water at a rate of 50 mgd utilizing source water at an average ocean salinity of 33.5 ppt. Applying this function to the historical variations in power plant flow rate and ocean salinity (Figure 1) generates the histogram in Figure 25, showing end-of-pipe salinities for the 50 mgd desalination plant (red) contrasted with those defining the natural variability of the ocean salinity (blue). Also shown in Figure 25 are dashed vertical lines showing the end-of-pipe salinities for the Unit 4 historical extreme cases (green). We find that the median end-of-pipe salinity from these historic variations would be only 36.8 ppt, while only about 2% of the outcomes would exceed the Unit 4 historical extreme of 40.11 ppt. Thus, the proposed operating scenario will not result in a significant salinity impact in the receiving water.

Figure 26 gives a histogram (red) and cumulative probability (blue) for the maximum sea floor salinity modeled at the edge of the ZID from the 20-yr records of the 7 controlling variables in Figures 1 and 4. The 2 % of historical flow rates less than 304 mgd (producing end-of- pipe salinites exceeding 40.11 ppt) were augmented by an assumption of supplemental pumping to bring flow rate up to the Unit-4 minimum of 304 mgd. Under these conditions we find that the median outcome is 34.4 ppt on the sea floor, identically the result from matching

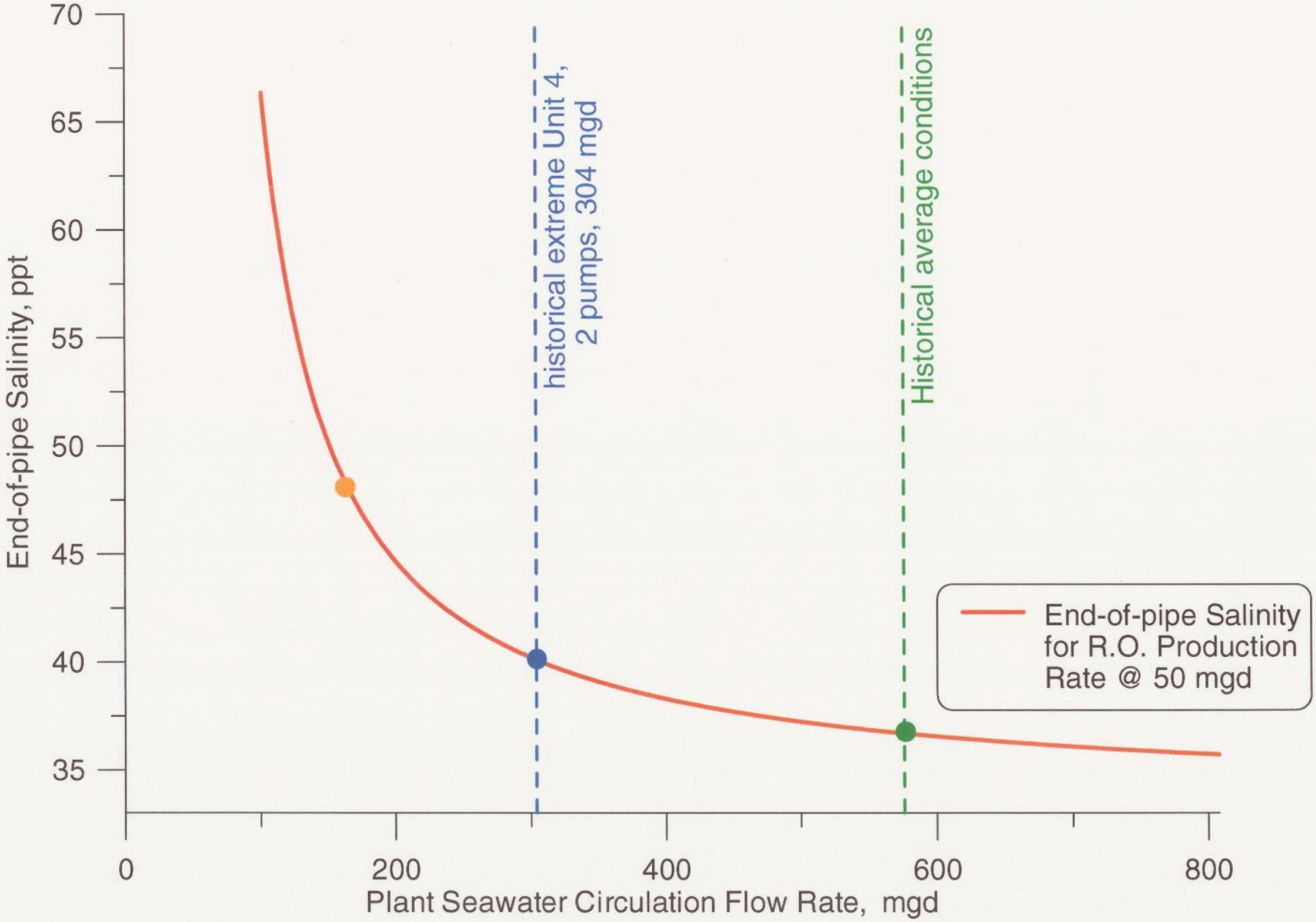

Figure 24. Sensitivity analysis of end-of-pipe salinity for Poseidon's desalination project at Encina Power Plant, Carlsbad, CA. Flow rates for model scenarios are shown at intersections with vertical dashed lines.

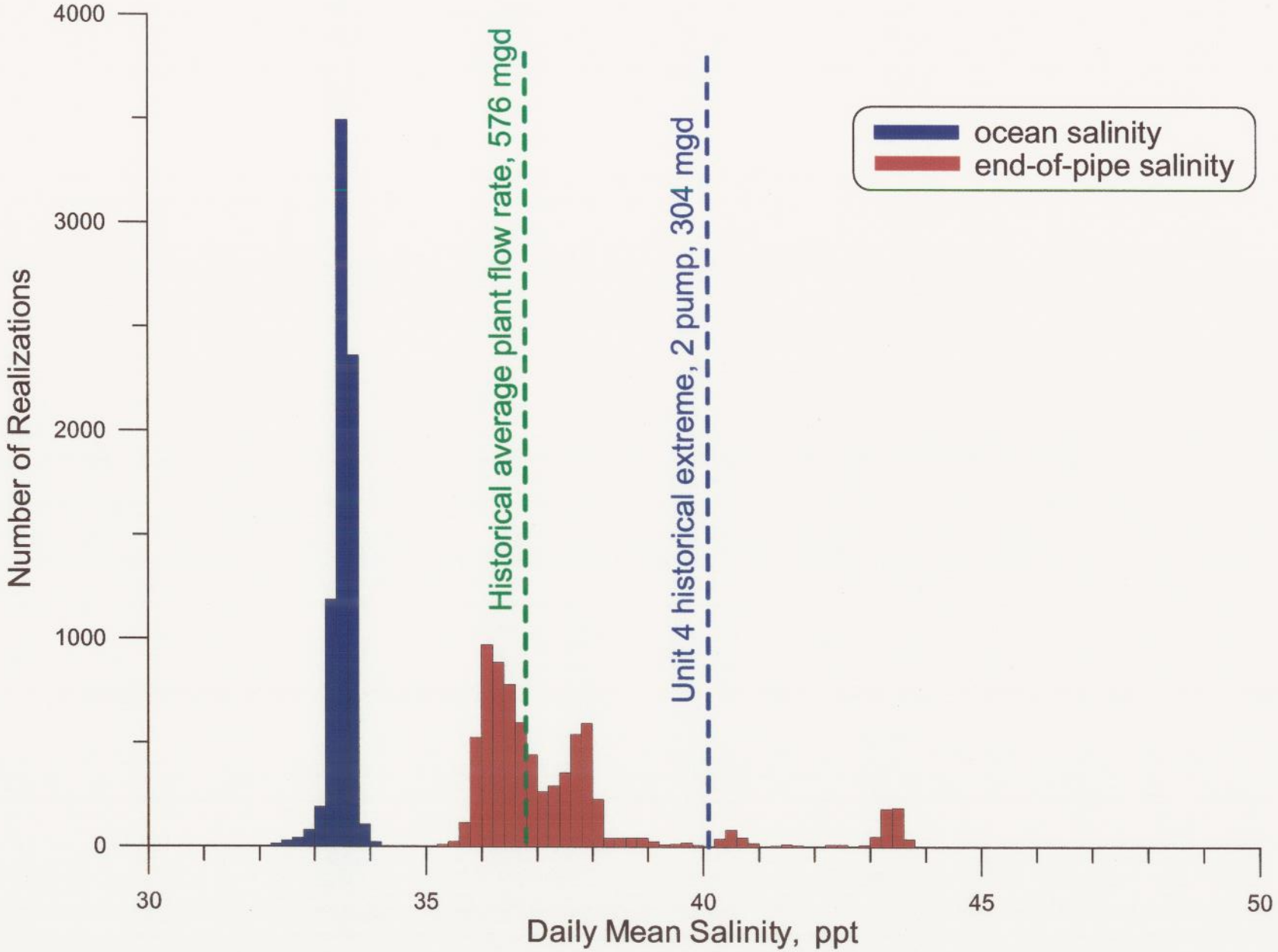

Figure 25. Comparison of histograms for daily mean ocean salinity vs end-of-pipe salinity based on historic ocean observations and Encina daily plant flow rates, 1980-2000. Ocean salinity off Encina (blue) and end-of-pipe combined discharge salinity for desalination plant producing at 50 mgd (red). Vertical dashed lines give end-of-pipe salinities for historicalical extreme model scenarios and scenario of historical average plant flow rate.

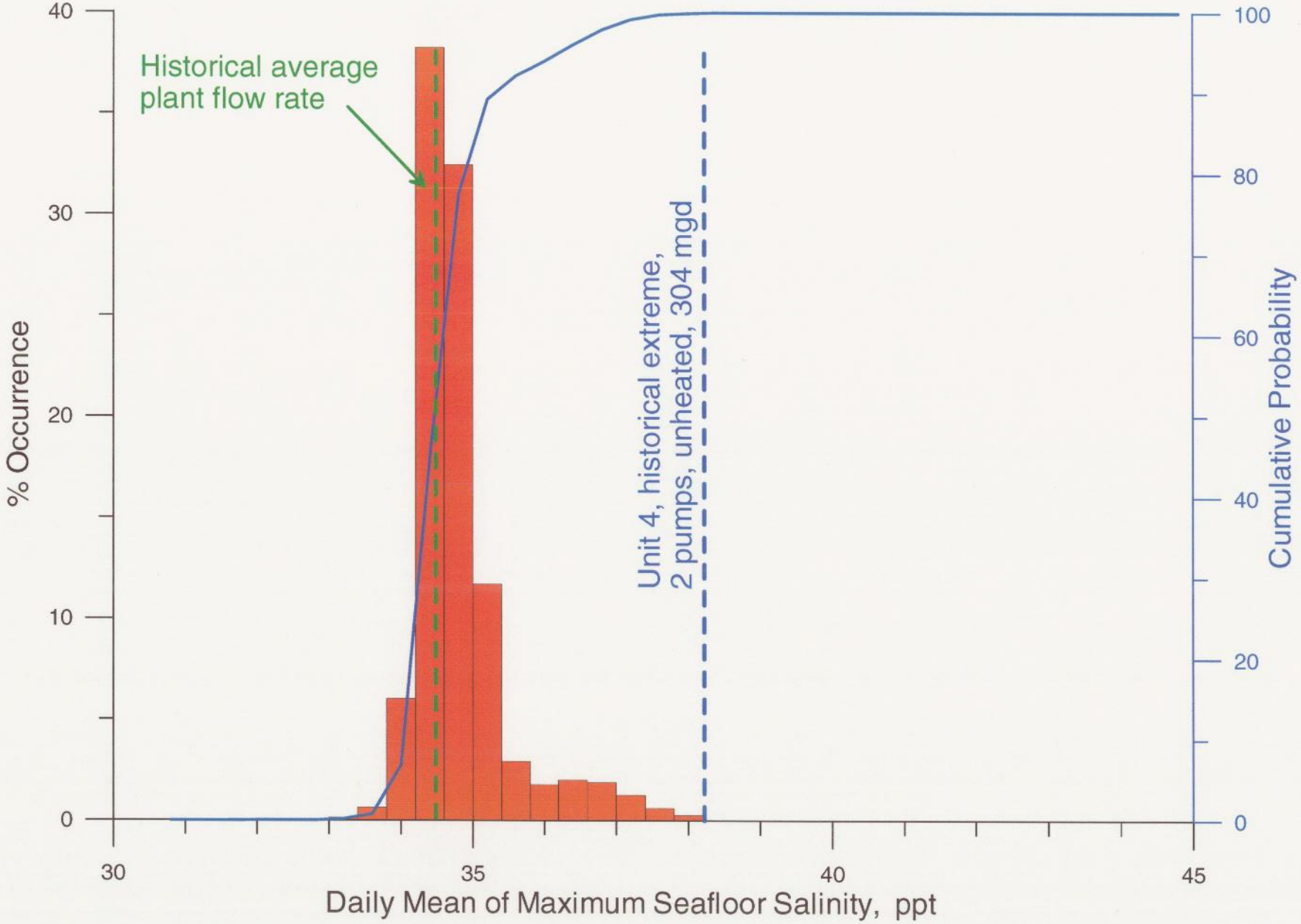

Figure 26. Histogram of maximum seafloor salinity at 1000 ft from the discharge (outer edge of zone of initial dilution, ZID). Model results based on desalination at 50 mgd with a 40 ppt limit on end-of-pipe salinity applied to historic observations of Encina daily plant flow rates, ocean mixing, and water mass properties, 1980-2000. Vertical dashed lines give salinities at ZID for historical extreme model scenarios and average plant flow rate scenario.

historical average power plant flow rates with the historically averaged ocean mixing conditions, as modeled in Figure 18. A bottom salinity of 34.4 ppt is also the maximum seasonal limit that occurs naturally in the local ocean. Therefore, it can be concluded that the saline impacts at the edge of the ZID will on average be within the seasonal maximums for ocean salinity at this site. Also, Figure 26 indicates that 95% of the time salinity at the edge of the ZID is less than 36.2 ppt and will never exceed 38.2 ppt, the Unit-4 limit.

We find a similar result in the dilution factors of the raw concentrate on the sea floor shown in Figure 27, presented in histogram form with corresponding cumulative probability. The median outcome is a minimum sea floor dilution factor of 29 to 1 based on the historical sequence of operational and environmental variables. However the potential range of minimum bottom dilution at the ZID goes as high as 96 to 1, and as low as 8 to 1, depending on the historical combinations of power plant operations and ocean mixing levels. Only 7 % of the potential outcomes produce dilutions of less than 15 to 1 at the edge of the ZID. The unheated Unit 4 historical extreme case for 304 mgd, gives a minimum bottom dilution at the ZID of 7.1 to 1.

From these results we can draw guidance for deciding the minimum power plant flow rate suitable for operating a 50 mgd desalination plant. Figure 28 shows the maximum sea floor (red) and water column (green) salinities at the edge of the ZID when the discharge is heated. Figure 29 gives a complementary set of curves for unheated discharge. We find that a power plant flow rate of at least 220 mgd will satisfy existing regulatory constraints that place a minimum water column dilution at the ZID of 15 to 1 (corresponding to a water column salinity of 35.74

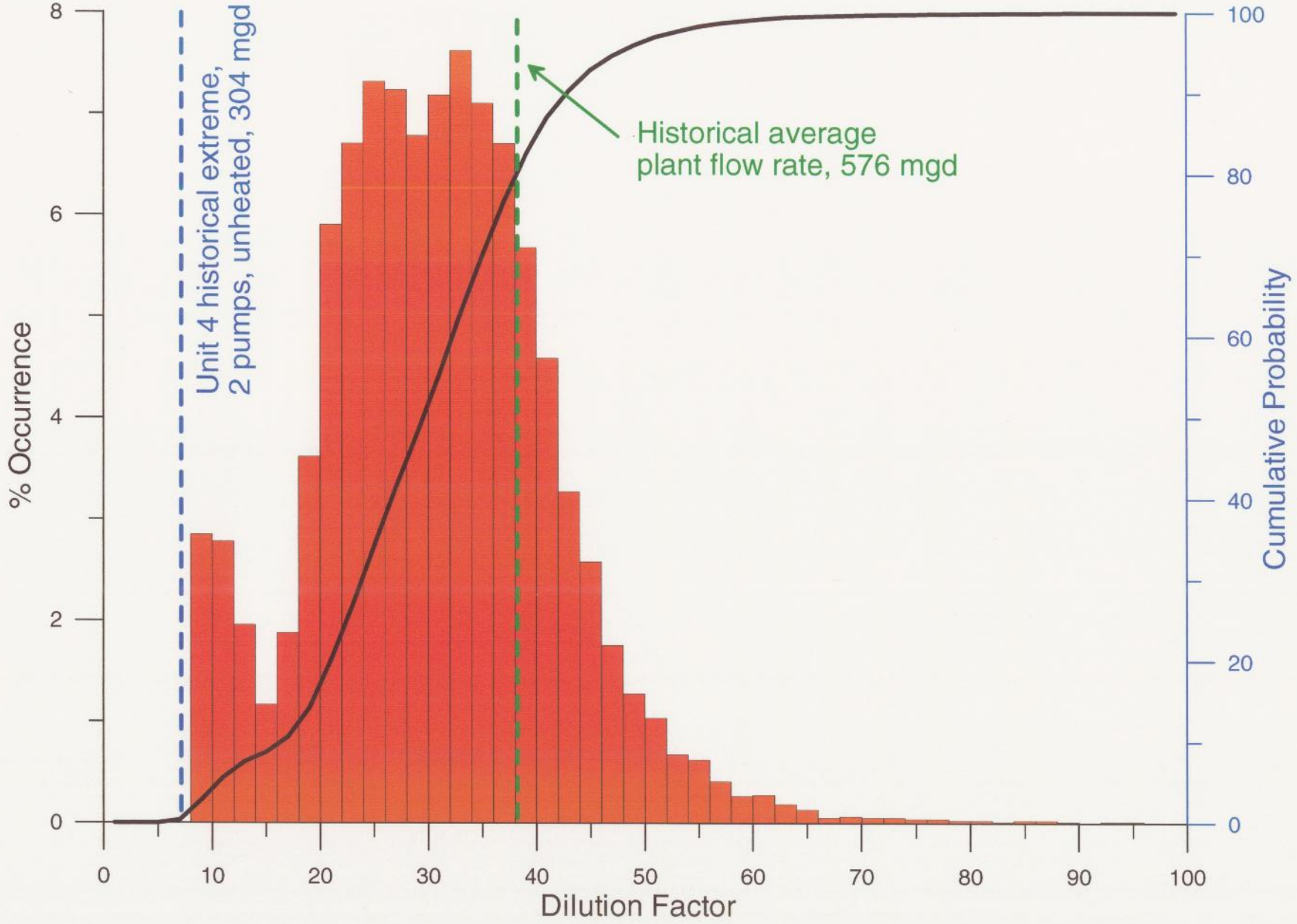

Figure 27. Histogram of minimum dilution on the seafloor at 1000 ft from the discharge (outer edge of zone of initial dilution, ZID). Model results based on desalination at 50 mgd with a 40 ppt limit on end-of-pipe salinity applied to historic observations of Encina daily plant flow rates, ocean mixing, and water mass properties, 1980-2000. Vertical dashed lines give bottom dilution at ZID for historical extreme model scenarios and historical average plant flow rate.

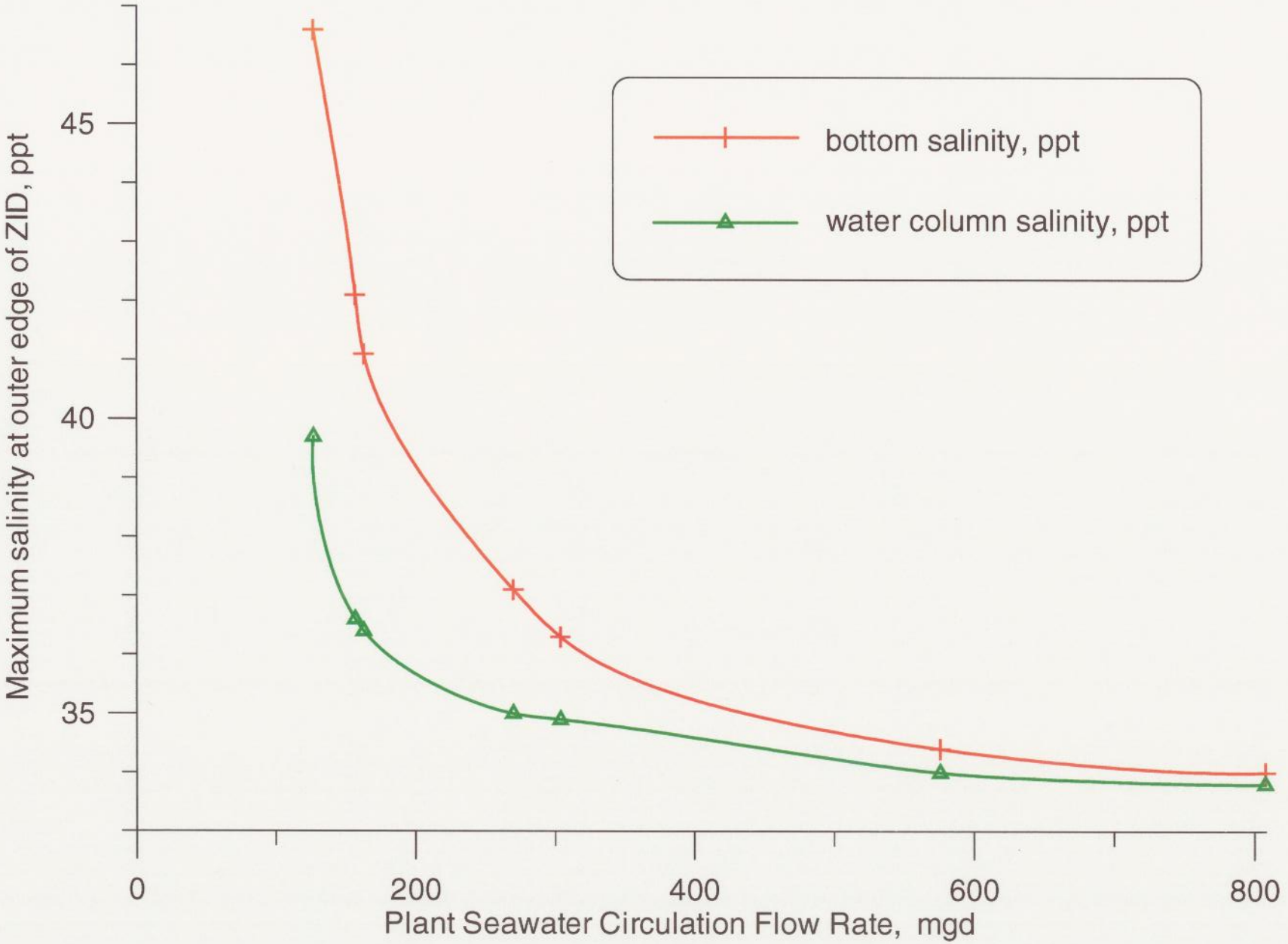

Figure 28. Sensitivity analysis of maximum salinity at 1000 feet from the discharge (outer edge of Zone of Initial Dilution, ZID) as a function of heated ($\Delta T = 5.5\ ^{o}C$) plant flow rate for Poseidon's desalination project at Encina Power Plant, Carlsbad, CA.

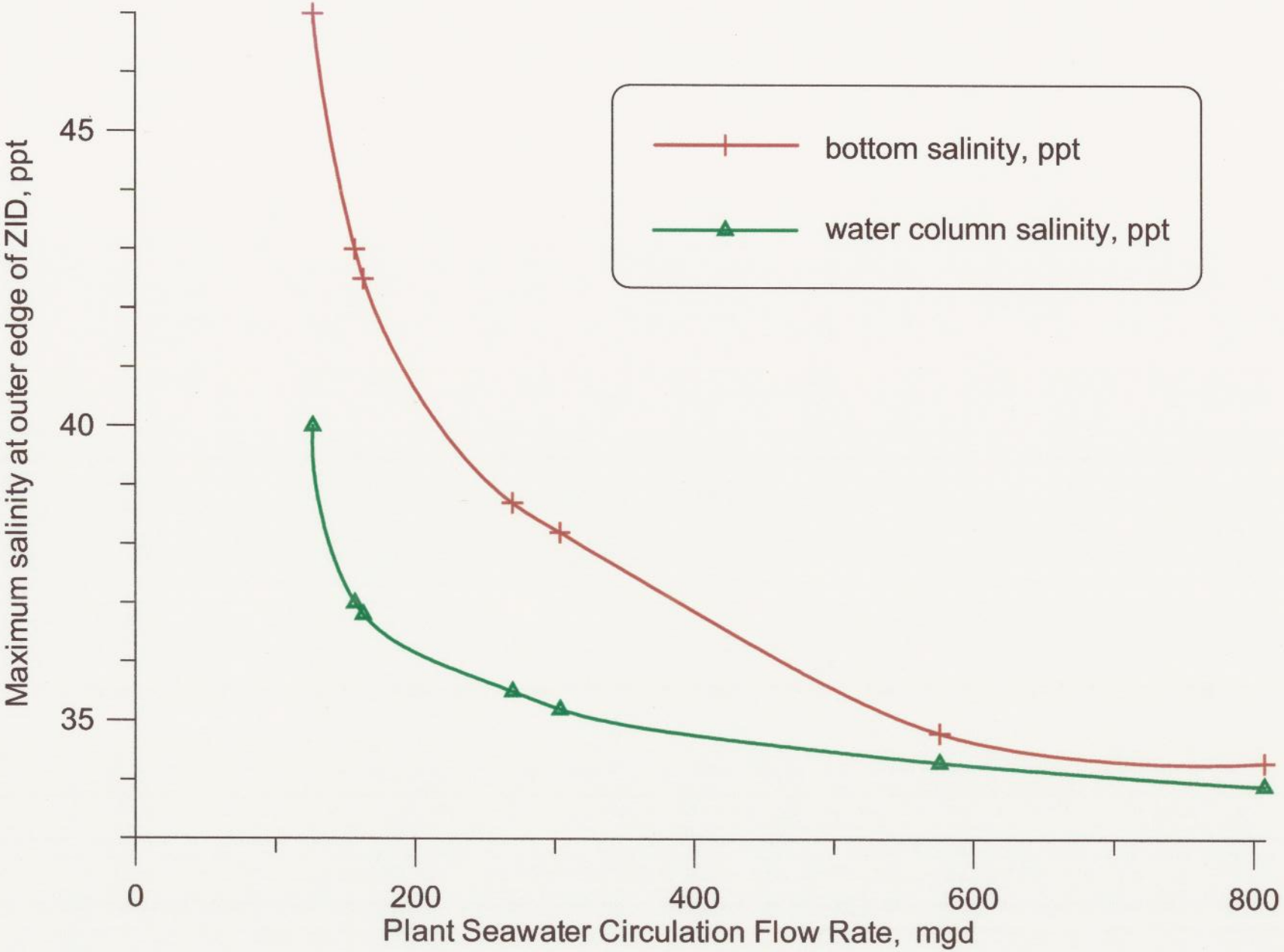

Figure 29. Sensitivity analysis of maximum salinity at 1000 feet from the discharge (outer edge of Zone of Initial Dilution, ZID) as a function of un-heated ($\Delta T = 0\ ^{o}C$) plant flow rate for Poseidon's desalination project at Encina Power Plant, Carlsbad, CA.

ppt). This criteria can be satisfied by requiring a minimum in-the pipe dilution for the concentrated sea water of 3.4 to 1. Furthermore the application of such standards to satisfy target levels at the outer edge of ZID is quite viable from a perspective of spacial variability. Figure 30 shows the histogram of the maximum sea floor salinity in the middle interior of the ZID, only 500 ft from the discharge channel. We find that all historically realizable outcomes with the 40.11 ppt limit at end-of-pipe (Unit-4 historic extreme scenario) produce bottom salinities less than 39 ppt and that 95 % of all potential outcomes are less than 37.8 ppt.

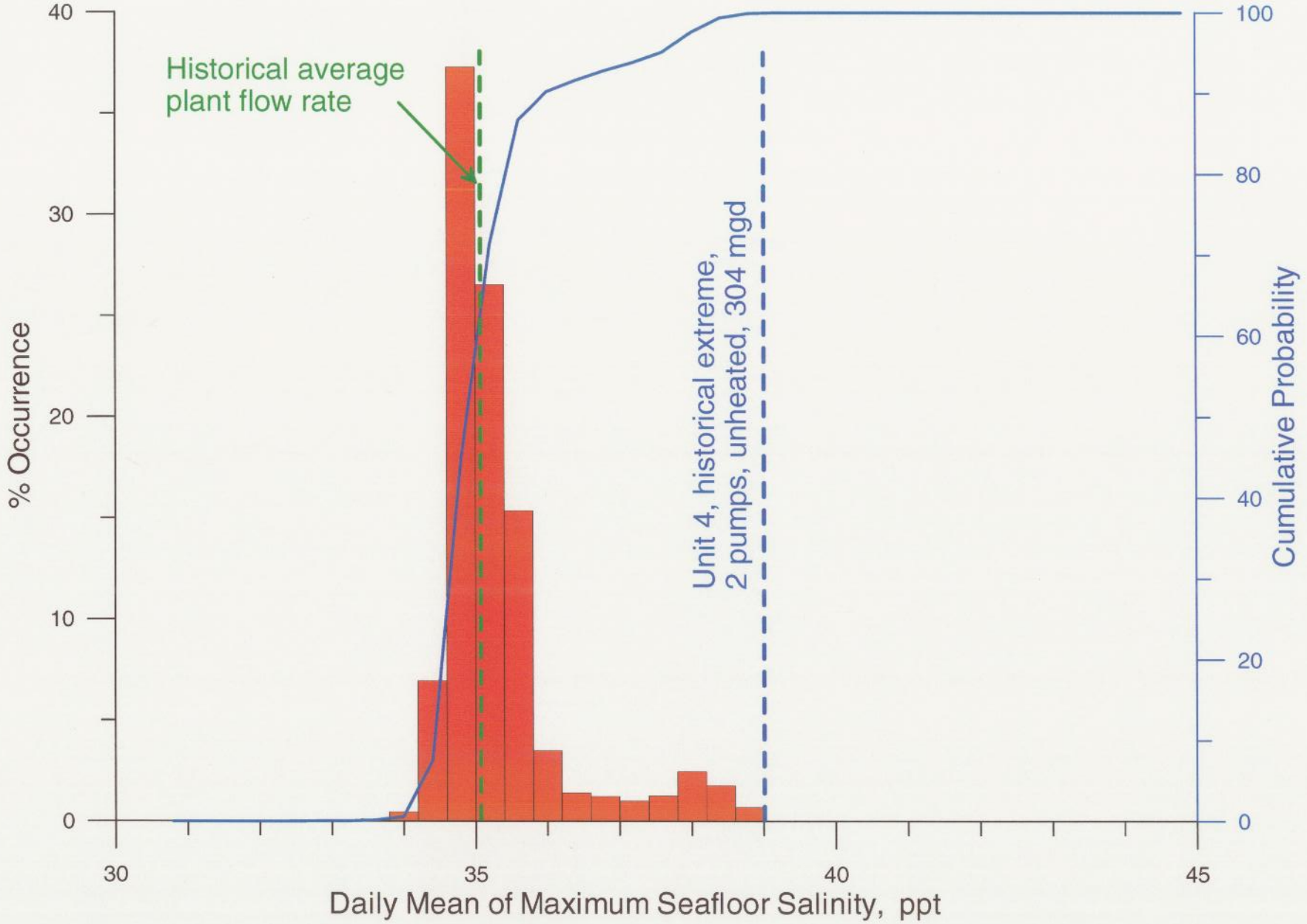

Figure 30. Histogram of maximum seafloor salinity at 500 ft from the discharge (middle of zone of initial dilution, ZID). Model results based on desalination at 50 mgd with a 40 ppt limit on end-of-pipe salinity applied to historic observations of Encina daily plant flow rates, ocean mixing, and water mass properties, 1980-2000. Vertical dashed lines give salinities inthe middle of the ZID for historical extreme model scenarios and average plant flow rate scenario.

5) Summary and Conclusions:

We have revisited the Part I analysis to examine in greater detail the notion of what was referred in that earlier study as "worst case" scenarios. In the present study we have considered certain "historical extremes" that involve some potential situations for operating the desalination plant when the power plant is not generating electricity or when it is operating at very low production levels that are either rare or atypical of the long-term historic operating envelope. We refer to these as "historical extreme cases" because they are caused by extreme conditions occurring "in-the-pipe" in combination with extreme conditions in the ocean environment. The extreme in-the-pipe conditions are due to either low power plant flow rate or no heating of the discharge water because the power plant is out of service. (The latter is referred to as "***Zero Delta-T***", $\Delta T = 0$, where ΔT is the temperature difference between ocean water and plant discharge). In the present study, these historical extreme conditions are superimposed on the historic extreme combinations of the remaining 6 controlling variables used previously in the Part I study. The resulting modeled response gives the expected impacts for a set of historical extreme cases that can not be reproduced from the historic records of all 7 controlling variables during last two decades (1980- July 2000). To establish a statistical comparison for these historical extreme cases, we find 7523 alternative solutions for the modeled ocean response to the 50 mgd desalination plant, based on historically realized plant operations and ocean conditions.

We evaluated 2 historical extreme case scenarios from which the desalination plant might extract its source water: 1) ***Unheated Unit 4 Historical Extreme Case*** with two circulation pumps and service water producing a total

flow rate 304 mgd and $\Delta T = 0$ °C; and, 2) ***Heated Unit 4 Historical Extreme Case*** with two circulation pumps and service wielding a flow rate of 304 mgd and $\Delta T =$ 5.5 °C. These historical extreme cases are contrasted against the historical average operating conditions with various combinations of pumps and service water producing 576 mgd of heated flow with $\Delta T = 5.5$ °C.

The analysis of these historical extreme case scenarios employed the ***SEDXPORT*** modeling system that was developed at Scripps Institution of Oceanography for the US Navy's *Coastal Water Clarity System* and *Littoral Remote Sensing Simulator*. This model has been peer reviewed multiple times and has been calibrated and validated in the Southern California Bight for 4 previous desalination design projects.

Results for the historical extreme case scenarios are summarized in Table 2 in terms of the maximum salinities and minimum dilution factors found on the sea floor and in the water column along the outer edge of the zone of initial dilution (ZID), 1000 feet from the discharge channel. In all cases the maximum salinities are found on the sea floor directly offshore of the discharge channel. Maximum salinities in the water column are found in the surf zone, down-drift from the discharge channel to the south. We find that both heated and unheated water discharges for the Unit 4 historical extreme scenarios appear to give acceptable dilution factors at the ZID ranging from 19.8 to 1 for the unheated discharges ($\Delta T = 0$ °C), increasing to 24.1 to 1 for the heated discharges ($\Delta T = 5.5$ °C). For historical average power plant operating conditions with heated discharge, the

dilution of the concentrated seawater from desalination is significantly higher than these historical extreme cases, reaching a minimum of 68.4 to 1 at the ZID.

Table 2. Summary of historical extreme case scenarios: salinity and dilution factors 1000 ft. from the discharge (outer edge of the zone of initial dilution, ZID).

Scenario	Plant Inflow rate (mgd)	Bottom salinity (ppt)	Bottom Dilution Factor	Water Column Salinity (ppt)	Water Column Dilution Factor
Unit 4 Historical Extreme (2 pumps, unheated)	304 ($\Delta T = 0$ °C)	38.2	7.1 to 1	35.2	19.8 to 1
Unit 4 Historical Extreme (2 pumps, heated)	304 ($\Delta T = 5.5$ °C)	36.3	12.0 to 1	34.9	24.1 to 1
Historical Average (variable pumps, heated)	576 ($\Delta T = 5.5$ °C)	34.4	37.7 to 1	34.0	68.4 to 1

When the model was run on 20.5 years of continuous historic data from the period 1980-July 2000. Figure 26 shows that maximum bottom salinity at the ZID varies from a minimum of 33 ppt to as high as 38.2 ppt, with a median value of

34.4 ppt (average ocean salinity is 33.5 ppt and seasonal maximum is 34.44). Figure 26 indicates that 95% of the time salinity at the edge of the ZID is less than 36.2 ppt and will never exceed 38.2 ppt, the Unit-4 limit for extreme historical cases. Because the concentrated seawater from desalination is heavier than ambient seawater, these bottom salinities represent the highest possible values found anywhere in the local marine environment during historical variability. In the middle of the ZID, only 500 ft from the discharge channel, the maximum sea floor salinities would remain less than 39.3 ppt for all possible outcomes within the realm of historical variability in ocean and power plant operating conditions. Figure 27 shows that the potential range of minimum bottom dilution at the ZID goes as high as 96 to 1, and as low as 8 to 1, depending on the historical combinations of power plant operations and ocean mixing levels. Only 7 % of the potential outcomes produce dilutions of less than 15 to 1 at the edge of the ZID. The unheated Unit 4 historical extreme case for 304 mgd, that provides a combined discharge of 254 mgd from the power plant and desalination plant, gives a minimum bottom dilution at the ZID of 7.1 to 1.

Based on these findings we conclude that the proposed Carlsbad Desalination Project when operated at a production level of 50 mgd and at power plant intake flow rates of 304 mgd or greater would produce a saline discharge that is everywhere less than 39 ppt; and thermal effects that are compliant with Water Quality Objectives under California's Thermal Plan. This suggests that a simple limit on end-of-pipe salinity at 40 ppt (as provided by a power plant intake flow rate limit of 304 mgd) would result in no significant impact in the receiving water.

6) Bibliography

Armi, L. A., 1979, "Effects of variations in eddy diffusivity on property distributions in the oceans," *Jour. of Mar. Res.*, v. 37, n. 3, p. 515-530.

Berkoff, J. C. W., 1972, "Computation of combined refraction-diffraction," *Proc. 13th Coastal Eng. Conf.*, p. 471-490.

Boas, M. L., 1966, *Mathematical Methods in the Physical Sciences,* John Wiley & Sons, Inc., New York, 778 pp., 1966.

Connor, J. J. and J. D. Wang, 1973, "Finite element modeling of two-dimensional hydrodynamic circulation," MIT Tech Rpt., #MITSG 74-4, p. 1-57.

Conte, S. D. and C. de Boor, 1972, *Elementary Numerical Analysis*, Second Edition, McGraw-Hill Book Co., New York.

CDIP (2001), "Coastal data information program," *SIO Reference Series*, 01-20 and http://cdip.ucsd.edu.

Durst, C. S., 1924, "The relationship between current and wind," *Quart. J. R. Met. Soc.*, v. 50, p. 113 (London).

deGroot, S. R. & P. Mazur, 1984, *Non-Equilibrium Thermodynamics,* Dover Pub., Inc., New York, 510 pp., 1984.

Dalrymple, R. A., J. T. Kirby and P. A. Hwang, 1984, "Wave diffraction due to areas of energy dissipation," *Jour. Waterway Port, Coast, and Ocean Engineering*, v. 110, p. 67-79.

Durst, C. S., 1924, "The relationship between current and wind," *Quart. J. R. Met. Soc.*, v. 50, p. 113 (London).

EA Engineering, Science, and Technology, 1997, "Encina Power Plant supplemental 316(a) assessment report," prepared for *San Diego Gas & Electric,* 101 Ash St., San Diego, CA 92112-4150, Report 60971.01.0002, p. 1-1-7-1.

Elwany, M. H. S., A. L. Lindquist, R. E. Flick, W. C. O'Reilly, J. Reitzel and W. A. Boyd, 1999, "Study of Sediment Transport Conditions in the Vicinity of Agua Hedionda Lagoon," submitted to California Coastal Commission, San Diego Gas & Electric, City of Carlsbad.

Finlayson, B. A., 1972, *The Method of Weighted Residuals and Variational Principles*, Academic Press.

Flick, R. E., R. T. Guza and D. L. Inman, 1981, "Elevation and velocity measurements of laboratory shoaling waves," *J. Geophys. Res.,* 86(C5), 4149-4160.

Flick, R. E. and E. H. Sterrett, 1994, "The San Diego Shoreline, Shoreline Erosion Assessment and Atlas of the San Diego Region," Vol. 1, *California Department of Boating and Waterways*, 135 pp.

Gallagher, R. H., 1981, *Finite Elements in Fluids*, John Wiley & Sons, New York, 290 pp.

Goddard, L. and Graham, N.E. 1997, "El Niño in the 1990's" *Jour. Geophysical Res.*, v. 102, n. C5, p. 10,423-36.

Hammond, R. R., S. A. Jenkins, J. S. Cleveland, J. C. Talcott, A. L. Heath, J. Wasyl, S. G. Goosby, K. F. Schmitt and L. A. Leven, 1995, "Coastal water clarity modeling," *SAIC*, Tech. Rpt. 01-1349-03-4841-000, 491 pp.

Inman, D. L. and S. A. Jenkins, 1983, "Oceanographic Report for Oceanside Beach Facilities," prepared for *City of Oceanside,* Oceanside, California, August, 1983, 206 pp.

Inman, D. L. and S. A. Jenkins, 1985, "Erosion and accretion waves from Oceanside Harbor," p. 591-3 in *Oceans 85: Ocean Engineering and the Environment*, Marine Technological Society & IEEE, v. 1, 674 pp.

Inman, D. L. and Masters, P. M., 1991, "Coastal sediment transport concepts and mechanisms," Chapter 5 (43 pp.) in *State of the Coast Report, San Diego Region, Coast of California Storm and Tidal waves Study*, U. S. Army Corps of Engineers, Los Angeles District Chapters 1-10, Appen. A-I, 2 v.

Inman, D. L. and P. M. Masters, 1991, "Budget of sediment and prediction of the future state of the coast," Chapter 9 (105 pp.) in *State of the Coast Report, San Diego Region, Coast of California Storm and Tidal Waves Study*, U. S. Army Corps of Engineers, Los Angeles District, Chapters 1-10, Appen. A-I; 2 v.

Inman, D. L., M. H. S. Elwany and S. A. Jenkins, 1993, "Shorerise and bar-berm profiles on ocean beaches, *Jour. Geophys. Res.,* 98(C10), p. 18, 181-199.

Inman, D. L. and S. A. Jenkins, 1996, "A chronology of ground mine studies and scour modeling in the vicinity of La Jolla," *University of California, San Diego*, Scripps Institution of Oceanography, SIO Reference Series 96-13, 26 pp.

_____S. A. Jenkins and M. H. S. Elwany, 1996, "Wave climate cycles and coastal engineering practice," *Coastal Engineering, 1996, Proc. 25th Int. Conf., (Orlando)*, ASCE, New York, v. 1, Ch 25, p. 314-27.

_____and S. A. Jenkins, 1997, "Changing wave climate and littoral drift along the California coast," p. 538-49 in O. T. Magoon et al., eds., *California and the World Ocean '97*, ASCE, Reston, VA, 1756 pp.

Inman, D. L., C. E. Nordstrom & R. E. Flick, 1976, "Currents in submarine canyons: an air-sea-land interaction," p. 275-310 in M. Van Dyke, et al (eds.), *Annual Review of Fluid Mechanics,* v. 8, 418 pp.

Jenkins, S. A., and J. Wasyl, 2001, "Agua Hedionda Lagoon north jetty restoration project: sand influx study", Tech. Rpt., submitted to Cabrillo Power, 1LLC, 178 pp. + app.

Jenkins, S. A. & J. Wasyl, 2001, "HYDRODYNAMIC MODELING OF DISPERSION AND DILUTION OF CONCENTRATED SEAWATER PRODUCED BY THE OCEAN DESALINATION PROJECT AT THE ENCINA POWER PLANT, CARLSBAD, CA", submitted to Poseidon Resources, 210 pp.

Jenkins, S. A. & J. Wasyl, 1994, "Numerical modeling of the tidal hydraulics and inlet closures at Agua Hedionda Lagoon, Part II: risk analysis," submitted to *SDG&E,* 60 pp.

Jenkins, S. A. & J. Wasyl, 1993, "Numerical modeling of tidal hydraulics and inlet closures at Agua Hedionda Lagoon," submitted to *SDG&E,* 91 pp.

Jenkins, S. A. and D. L. Inman, 1985, "On a submerged sphere in a viscous fluid excited by small amplitude periodic motion," *Jour. Fluid Mech.*, v. 157, p. 199-124.

_____and J. Wasyl, 1990, "Resuspension of estuarial sediments by tethered wings," *Jour. of Coastal Res.*, v. 6, n. 4, p. 961-980.

Jenkins, S. A., S. Aijaz and J. Wasyl, 1992, "Transport of fine sediment by hydrostatic jets," *Coastal and Estuarine Studies, American Geophysical Union*, v. 42, p. 331-47.

Jenkins, S. A. & D. W. Skelly, 1989, "An evaluation of the coastal data base pertaining to seawater diversions at Encina Power Plant," *SIO Reference Series,* #89-4, 52 pp.

Jenkins, S. A. D. W. Skelly, & J. Wasyl, 1989, "Dispersion and momentum flux study of the cooling water outfall at Agua Hedionda," *SIO Reference Series,* #89-17, 36 pp.

Jenkins, S. A., D. L. Inman and W. G. Van Dorn, 1981, "Evaluation of sediment management procedures," *University of California, San Diego*, Scripps Institution of Oceanography, SIO Reference Series No. 81-22, 212 pp.

Kirby, J. T., 1986a, "Higher-order approximations in the parabolic equation method for water waves," *Jour. Geophys. Res.*, v. 91, C1, p. 933-952.

_____, 1986b, "Rational approximations in the parabolic equation method for water waves," *Coastal Engineering*, 10, p. 355-378.

_____, 1986c, "Open boundary condition in the parabolic equation method," *Jour. Waterway, Port, Coastal, and Ocean Eng.*, 112(3), p. 460-465.

Komar, P. D. and D. L. Inman, 1970, "Longshore sand transport of beaches," *Jour. Geophys. Res.*, v. 75, n. 30, p. 5914-5927.

Lazara, B. J. and J. C. Lasheras, 1992a, "Particle dispersion in a developing free shear layer, Part 1, Unforced flow," *Jour. Fluid Mech.* 235, p. 143-178.

Lazara, B. J. and J. C. Lasheras, 1992b, "Particle dispersion in a developing free shear layer, Part 2, Forced Flow," *Jour. Fluid Mech.*, 235, p. 179-221.

LePage, S. and R. Ware, 2001, "Assessment of biological impacts of the Agua Hedionda jetty restoration project", Tech. Rpt. Submitted to Cabrillo Power 1LLC.

List, E. J., G. Gartrell and C. D. Winant, 1990, "Diffusion and dispersion in coastal waters," *Jour. Hydraulic Eng.*, v. 116, n. 10, p. 1158-79.

Longuet-Higgins, M. S., 1970, "Longshore currents generated by obliquely incident waves," *Jour. Geophys. Res.*, v. 75, n. 33, p. 6778-6789.

Martin, J. E. and E. Meiberg, 1994, "The accumulation and dispersion of heavy particles in forced two-dimensional mixing layers, 1: The fundamental and subharmonic cases," *Phys. Fluids*, A-6, p. 1116-1132.

Neumann, G., 1952, "Ober die komplexe Natur des Seeganges, Teil 1 and 2," *Deut. Hydrogr. Zeit.*, v. 5, n. 2/3, p. 95-110, n. 5/6, p. 252-277.

_____and W. J. Pierson, Jr., 1966, *Principles of Physical Oceanography*, Prentice-Hall, Inc., Englewood Cliffs, NJ, 545 pp.

Nielsen, P., 1979, "Some basic concepts of wave sediment transport," Series Paper No. 20, *Institute of Hydrodyn. and Hydro. Eng., Tech. Univ. of Denmark.*

NOAA, 2000, "Verified/Historical Water Level Data" http://www.opsd.nos.noaa.gov/data_res.html

Oden, J. T. and E. R. A. Oliveira, 1973, *Lectures on Finite Element Methods in Continuum Mechanics*, The University of Alabama Press.

Pawka, S. S., D. L. Inman, R. L. Lowe & L. Holmes, 1976, "Wave climate at Torrey Pines Beach, California," *U. S. Army Corps of Engineers,* Coastal

Engineering Research Center, Tech Paper 76-5, 372 pp.

Pawka, S. S., 1982, "Wave directional characteristics on a partially sheltered coast", PhD dissertation, University of California, San Diego, 246 pp.

Radder, A. C., 1979, "On the parabolic equation method for water-wave propagation," *J. Fluid Mech.*, 95, part 1, p. 159-176.

Schmidt, W., 1917, "Wirkungen der ungeordneten Bewegungen im Wasser der Meere und Seen," *Ann. D. Hydr. u. Marit. Meteorol.*, vol. 45, p. 367-381.

Schoonmaker, J. S., R. R. Hammond, A. L. Heath and J. S. Cleveland, 1994, "A numerical model for prediction of sub-littoral optical visibility," *SPIE Ocean Optics XII*, 18 pp.

SIO, 2001, "SIO shore station, Scripps Pier", http://www-mlrg.ucsd.edu/shoresta/mnSIOMain/siomain.htm

Stommel, H., 1949, "Horizontal diffusion due to oceanic turbulence," *Journal of Marine Research*, v. VIII, n. 3, p. 199-225.

Thorade, H., 1914, "Die Geschwindigkeit von Triftstromungen und die Ekman'sche Theorie," *Ann. D Hydr. u. Marit. Meteorol.*, v. 42, p. 379.

Schmidt, W., 1917, "Wirkungen der ungeordneten Bewegungen im Wasser der Meere und Seen," *Ann. D. Hydr. u. Marit. Meteorol.*, vol. 45, p. 367-381.

Schoonmaker, J. S., R. R. Hammond, A. L. Heath and J. S. Cleveland, 1994, "A numerical model for prediction of sub-littoral optical visibility," *SPIE Ocean Optics XII*, 18 pp.

Wang, H. P., 1975, "Modeling an ocean pond: a two-dimensional, finite element hydrodynamic model of Ninigret Pond, Charleston, Rhode Island," *Univ. of Rhode Island, Marine Tech. Rpt.*, #40, p. 1-58.

Weiyan, T., 1992, *Shallow Water Hydrodynamics*, Water & Power Press, Hong Kong, 434 pp.

White, W. B. And Cayan, D.R. 1998, "Quasi-periodicity and global symmetries in interdecadal upper ocean temperature variability", *Jour. Geophysical Res.*, v. 103, n. C10, p. 21,335-54.

Winant, C. D., 1974, "Internal surges in coastal waters," *Jour. Geophys. Res.*, v. 79, n. 30, p. 4523-26.